ISET Journal of Earthquake Technology, Paper No. 489, Vol. 44, No. 2, June 2007, pp. 341–375

DIFFRACTION OF PLANE SV WAVES BY AN UNDERGROUND CIRCULAR CAVITY IN A SATURATED POROELASTIC HALF-SPACE

Jianwen Liang*, Zhenning Ba* and Vincent W. Lee**

*Department of Civil Engineering
Tianjin University, Tianjin 300072, China
**Department of Civil Engineering
University of Southern California, Los Angeles, CA 90089-2531, U.S.A.

ABSTRACT

This paper derives a wave-function series expansion solution for the diffraction of incident plane SV waves by an underground circular cavity in a saturated poroelastic half-space. The effects of the incident frequencies, incident angles, boundary drainage, porosity, and Poisson's ratio on the diffraction of incident plane SV waves are discussed. It is shown that, depending upon the incident angles, the surface displacement amplitudes near the cavity in dry and saturated poroelastic half-spaces are very different, and large phase shifts can be observed. The Poisson's ratio is also an important factor, and has a larger effect for the undrained saturated than for the drained saturated half-space. Large pore pressures are found near and around the cavity, depending strongly upon the incident angles. As the porosity increases the pore pressure increases significantly but its variations become smoother and more complicated as the frequency increases. For large porosity, the effect of the drainage condition is significant, and for the same porosity the surface displacement amplitudes near the cavity in the undrained are larger than those in the drained saturated half-space.

KEYWORDS: Poroelastic Half-Space Cavity, Fluid Saturation, Biot's Theory, Porosity, Drained and Undrained Boundary

INTRODUCTION

The response of an underground cavity to incident seismic waves is one of the important topics in earthquake engineering. It may be evaluated either by an analytical wave-function series expansion method or by numerical methods. Numerical methods may include, for example, the finite difference, finite element, boundary integral equation, or discrete wave number methods. The advantage of the numerical methods is that they can be applied to a cavity of arbitrary shape. However, analytical methods continue to be essential in exploring the physical nature of the problems, and also for checking the accuracy of the numerical methods. Analytical methods have been used to obtain solutions for a few simple elastic cases: circular tunnels excited by plane SH waves (Lee and Trifunac, 1979) and circular cavities excited by plane P and SV waves (Lee and Karl, 1992, 1993; Davis et al., 2001). All of these solutions have been obtained for the case of homogeneous elastic half-space.

Biot (1956a, 1956b, 1962) proposed a theory of wave propagation in a saturated poroelastic medium and demonstrated the existence of two compressive waves. The second P wave is generated by the relative motion between the solid and fluid phases. Many studies of wave propagation in saturated poroelastic media based on Biot's theory have been carried out—e.g., Berryman (1980, 1981, 1985), Deresiewicz (1960, 1961, 1962, 1964a, 1964b, 1965), Deresiewicz and Rice (1962, 1964), Deresiewicz and Skalak (1963), Deresiewicz and Wolf (1964), Deresiewicz and Levy (1967), Lin et al. (2005), Paul (1976a, 1976b), Philippacopoulos (1988, 1997, 1998), Prevost (1985, 1987), Santos (1986), Santos and Orena (1986), Santos et al. (1990, 1992), Senjuntichai and Rajakapse (1994), Theodorakopoulos et al. (2001a, 2001b, 2004), Theodorakopoulos (2003a, 2003b), Theodorakopoulos and Beskos (2003), Vardoulakis and Beskos (1986), Yang and Sato (2001), Zienkiewicz et al. (1980), and Zienkiewicz and Shiomi (1984). Lin et al. (2005) studied the effects of boundary drainage on wave propagation in a saturated half-space. However, it should be noted that to date there are few analytical solutions in the literature for cavities in a saturated poroelastic half-space.

Based on Biot's theory, this study presents an analytical solution for the diffraction of incident plane SV waves by an underground circular cavity in a saturated poroelastic half-space by using the wave-

function expansion method. The solutions are presented in terms of frequency, incidence angle, porosity, boundary drainage, and Poisson's ratio.

THE MODEL

The model considered in this paper consists of a circular cavity embedded in a saturated poroelastic half-space as shown in Figure 1. The problem to be solved is a plain-strain problem. The cavity is centered at O_1, with radius a, and at depth h below the half-space surface. Both the rectangular and polar coordinate systems, with centers at O_1, are defined and used. Let O be the point on the surface of the half-space directly above the center O_1 of the cavity. With O as the origin, another set of rectangular and polar coordinate systems can be defined.

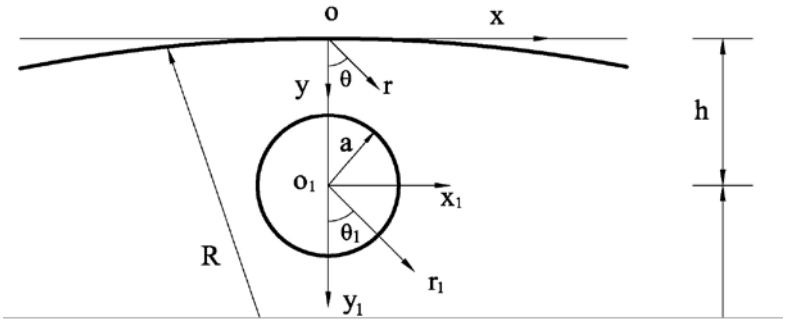

Fig. 1 The model

1. Biot's Theory of a Poroelastic Medium

Biot's wave equations are for a porous medium in which the solid frame is isotropic and elastic, and the pore fluid is allowed only to have dilatational deformation. Those equations can be expressed as follows (Biot, 1956a, 1956b; Deresiewicz, 1961):

$$\begin{aligned}(\lambda_{sat}+2\mu)\nabla^2\phi+Q\nabla^2\Phi&=\frac{\partial^2}{\partial t^2}\left(\rho_{11}\phi+\rho_{12}\Phi\right)+\hat{b}\frac{\partial}{\partial t}\left(\phi-\Phi\right)\\ Q\nabla^2\phi+R\nabla^2\Phi&=\frac{\partial^2}{\partial t^2}\left(\rho_{12}\phi+\rho_{22}\Phi\right)-\hat{b}\frac{\partial}{\partial t}\left(\phi-\Phi\right)\end{aligned} \tag{1}$$

$$\begin{aligned}\mu\nabla^2\psi&=\frac{\partial^2}{\partial t^2}\left(\rho_{11}\psi+\rho_{12}\Psi\right)+\hat{b}\frac{\partial}{\partial t}\left(\psi-\Psi\right)\\ 0&=\frac{\partial^2}{\partial t^2}\left(\rho_{12}\psi+\rho_{22}\Psi\right)-\hat{b}\frac{\partial}{\partial t}\left(\psi-\Psi\right)\end{aligned} \tag{2}$$

where ϕ and Φ are P-wave potentials for the dry frame and the pore fluid, respectively; ψ and Ψ are S-wave potentials for the dry frame and the pore fluid, respectively; λ_{sat}, μ, Q, and R are the elastic moduli for a saturated solid-fluid system; ρ_{11}, ρ_{12}, and ρ_{22} are the dynamic mass coefficients; and $\hat{b}$ is a dissipative coefficient. In a porous medium saturated with inviscid fluid, the wave equations become non-dissipative—i.e., $\hat{b}$ = 0, due to the lack of fluid viscosity.

The dynamic mass coefficients can be described as follows (Berryman, 1980):

$$\rho_{11} = (1-n)\rho_s + \hat{\gamma}(1-n)\rho_f \tag{3}$$

$$\rho_{12} = -\hat{\gamma}(1-n)\rho_f \tag{4}$$

$$\rho_{22} = n\rho_f + \hat{\gamma}(1-n)\rho_f \tag{5}$$

where n is the porosity, ρ_s is the density of the solid material, ρ_f is the density of the fluid, and $\hat{\gamma}$ is the coefficient for induced inertia by solid-fluid interaction, which depends upon the shape of the solid particles—e.g., $\hat{\gamma}$ = 0.5 for spherical particles (Berryman, 1980).

Biot and Willis (1957) correlated the elastic moduli with experimental measurements of porosity, compressibility of the solid grain, compressibility of the (solid) dry frame, and with compressibility of the fluid, in which shear strength of the porous material is provided by the frame and is not affected by saturation with the fluid ($\mu = \mu_{\text{dry}} = \mu_{\text{sat}}$). Thus, the elastic moduli can be expressed as

$$\mu = \frac{3(1-2\nu)}{2(1+\nu)} K_{\text{dry}} \tag{6}$$

$$\lambda_{\text{sat}} = \lambda_{\text{dry}} + \frac{Q^2}{R} = \frac{3\nu}{1+\nu} K_{\text{dry}} + \frac{\left(1-n-K_{\text{dry}}/K_g\right)^2}{\left(1-n-K_{\text{dry}}/K_g\right) + nK_g/K_f} K_g \tag{7}$$

$$Q = \frac{n\left(1-n-K_{\text{dry}}/K_g\right)}{\left(1-n-K_{\text{dry}}/K_g\right) + nK_g/K_f} K_g \tag{8}$$

$$R = \frac{n^2}{\left(1-n-K_{\text{dry}}/K_g\right) + nK_g/K_f} K_g \tag{9}$$

where μ is the shear modulus of the frame material or skeleton; λ_{dry} is its Lamé constant; ν is its Poisson's ratio; and K_{dry} is its bulk modulus, with

$$K_{\text{dry}} = K_{\text{cr}} + (1-n/n_{\text{cr}})\left(K_g - K_{\text{cr}}\right) \tag{10}$$

Further, K_g is the bulk modulus of solid grains, K_f is the bulk modulus of fluid, n_{cr} is the critical porosity, and K_{cr} is the critical bulk modulus of the frame material.

There are two P waves in the saturated medium, with their velocities given by (Deresiewicz, 1960)

$$c_{\alpha j} = \sqrt{\frac{2A}{B \mp \left(B^2 - 4AC\right)^{1/2}}}; \quad j = 1, 2 \tag{11}$$

where $A = PR - Q^2$, $P = \lambda_{\text{sat}} + 2\mu$, $B = \rho_{11}R + \rho_{22}P - 2\rho_{12}Q$, and $C = \rho_{11}\rho_{22} - \rho_{12}^2$.

The general solution of the P waves for the solid frame is

$$\phi = \phi_1 + \phi_2 \tag{12}$$

and that for the P waves of the pore fluid is

$$\Phi = \Phi_1 + \Phi_2 = f_1\phi_1 + f_2\phi_2 \tag{13}$$

where f_1 and f_2 are given by

$$f_j = \frac{A/c_{\alpha,j}^2 - \rho_{11}R + \rho_{12}Q}{\rho_{12}R - \rho_{22}Q}; \quad j = 1, 2 \tag{14}$$

The velocity of the S wave in the saturated medium is

$$c_\beta = \sqrt{\frac{\mu\rho_{22}}{C}} \tag{15}$$

and the general solution for the solid frame is

$$\Psi = f_3 \psi \tag{16}$$

with

$$f_3 = -\frac{\rho_{12}}{\rho_{22}} \tag{17}$$

2. The Incident, Reflected, and Scattered Waves

Consider an incident, plane SV wave with frequency ω and incident angle θ_β, which can be expressed in exponential form as

$$\psi^{(i)}(x,y) = \exp\left[\mathrm{i}k_\beta\left(x\sin\theta_\beta - y\cos\theta_\beta\right)\right] \tag{18}$$

with wavelength $\lambda_\beta = 2\pi/k_\beta$ and wave number $k_\beta = \omega/c_\beta$. Here, "i" is the imaginary unit. The time factor $\exp(-\mathrm{i}\omega t)$ is understood and is omitted here and henceforth.

In the presence of the half-space surface without the cavity, the reflected P_I waves, P_{II} waves, and SV waves are generated as a result of the incident SV wave, and their potential functions can be expressed, respectively, as (Lin et al., 2005)

$$\phi_1^{(r)}(x,y) = a_1 \exp\left[\mathrm{i}k_{\alpha 1}\left(x\sin\theta_{\alpha 1} + y\cos\theta_{\alpha 1}\right)\right] \tag{19}$$

$$\phi_2^{(r)}(x,y) = a_2 \exp\left[\mathrm{i}k_{\alpha 2}\left(x\sin\theta_{\alpha 2} + y\cos\theta_{\alpha 2}\right)\right] \tag{20}$$

$$\psi^{(r)}(x,y) = b \exp\left[\mathrm{i}k_\beta\left(x\sin\theta_\beta + y\cos\theta_\beta\right)\right] \tag{21}$$

where $k_{\alpha 1} = \omega/c_{\alpha 1}$ and $k_{\alpha 2} = \omega/c_{\alpha 2}$ are the wave numbers of the longitudinal P_I and P_{II} waves in the half-space, respectively, and a_1, a_2 and b are the reflection coefficients.

The incident SV wave (Equation (18)) and the reflected SV wave (Equation (21)) are combined and expanded into a Fourier-Bessel series as follows (Pao and Mow, 1973):

$$\psi^{(i+r)}(r_1,\theta_1) = \psi^i + \psi^r = \sum_{n=0}^{\infty} J_n\left(k_\beta r_1\right)\left(C_{0,n}\sin n\theta_1 + D_{0,n}\cos n\theta_1\right) \tag{22}$$

where

$$\begin{Bmatrix} C_{0,n} \\ D_{0,n} \end{Bmatrix} = \varepsilon_n \mathrm{i}^n \begin{Bmatrix} \sin n\theta_\beta \\ \cos n\theta_\beta \end{Bmatrix} \left[\mp(-1)^n \exp\left(-\mathrm{i}k_\beta h\cos\theta_\beta\right) + b\exp\left(\mathrm{i}k_\beta h\cos\theta_\beta\right)\right] \tag{23}$$

with $\varepsilon_n = 1$ and $\varepsilon_n = 2$ when $n \geq 1$.

There are two possible critical angles for the reflected P_I and P_{II} waves, respectively, in a poroelastic half-space (Lin et al., 2005):

$$\theta_{\mathrm{cr}1} = \sin^{-1}(c_\beta / c_{\alpha 1}) \tag{24}$$

$$\theta_{\mathrm{cr}2} = \sin^{-1}(c_\beta / c_{\alpha 2}) \tag{25}$$

Case I: The incident angle is less than the first critical angle—i.e., $\theta_\beta < \theta_{\mathrm{cr}1}$. Equation (19) can be expanded into a Fourier-Bessel series as follows:

$$\phi_1^{(r)}(r_1,\theta_1) = \sum_{n=0}^{\infty} J_n\left(k_{\alpha 1} r_1\right)\left(A_{01,n}\cos n\theta_1 + B_{01,n}\sin n\theta_1\right) \tag{26}$$

where

$$\begin{Bmatrix} A_{01,n} \\ B_{01,n} \end{Bmatrix} = \varepsilon_n \mathrm{i}^n \begin{Bmatrix} \cos n\theta_{\alpha 1} \\ \sin n\theta_{\alpha 1} \end{Bmatrix} a_1 \exp\left(\mathrm{i}k_{\alpha 1} h\cos\theta_{\alpha 1}\right) \tag{27}$$

Case II: The incident angle is greater than or equal to the first critical angle—i.e., $\theta_\beta \geq \theta_{\text{cr1}}$. When the incident angle reaches the first critical angle θ_{cr1}, the reflected P_I wave becomes a surface wave and propagates along the horizontal surface with its displacement amplitudes decreasing exponentially with depth (Lin et al., 2005). In this case,

$$\sin\theta_{\alpha 1} = \left(c_{\alpha 1}/c_\beta\right)\sin\beta > (c_{\alpha 1}/c_\beta)\sin\theta_{\text{cr1}} = 1 \tag{28}$$

and there is no real-valued solution for $\theta_{\alpha 1}$. There exists a real-valued quantity $\Phi_{\alpha 1}$ such that

$$1 < \left(c_{\alpha 1}/c_\beta\right)\sin\beta = \cosh\Phi_{\alpha 1} = \cos \mathrm{i}\Phi_{\alpha 1} = \sin(\pi/2 - \mathrm{i}\Phi_{\alpha 1}) = \sin\theta_{\alpha 1} \tag{29}$$

where $\theta_{\alpha 1} = (\pi/2) - \mathrm{i}\Phi_{\alpha 1}$ is a complex angle. Defining

$$k = k_{\alpha 1}\sin\theta_{\alpha 1} > k_{\alpha 1} \tag{30}$$

and

$$\gamma_1 = -\mathrm{i}k_{\alpha 1}\cos\theta_{\alpha 1} = -\mathrm{i}k_{\alpha 1}\sqrt{1-\sin^2\theta_{\alpha 1}} = \sqrt{k_{\alpha 1}^2\sin^2\theta_{\alpha 1} - k_{\alpha 1}^2} = \sqrt{k^2 - k_{\alpha 1}^2} > 0 \tag{31}$$

Equation (19) can be written as

$$\phi_1^{(r)}\left(r_1,\theta_1\right) = a_1\exp\left(-\gamma_1 h\right)\exp\left(\mathrm{i}k_{\alpha 1}r_1\cos\left(\theta_1 - \theta_{\alpha 1}\right)\right) \tag{32}$$

The contributions of ϕ_1^r to t_{rr}, $t_{r\theta}$, σ, U_r, and u_r are

$$P_{1t_{rr}}(r_1,\theta_1) = -\left(\left(\lambda + f_1 Q\right) + 2\mu\cos^2\left(\theta_1 - \theta_{\alpha 1}\right)\right)k_{\alpha 1}^2\phi_1^r \tag{33}$$

$$P_{1t_{r\theta}}(r_1,\theta_1) = \mu\sin 2(\theta_1 - \theta_{\alpha 1})k_{\alpha 1}^2\phi_1^r \tag{34}$$

$$P_{1\sigma}(r_1,\theta_1) = -(Q + f_1 r)k_{\alpha 1}^2\phi_1^r \tag{35}$$

$$P_{1u_r}(r_1,\theta_1) = \mathrm{i}\cos(\theta_1 - \theta_{\alpha 1})k_{\alpha 1}\phi_1^r \tag{36}$$

$$P_{1U_r}(r_1,\theta_1) = \mathrm{i}f_1\cos(\theta_1 - \theta_{\alpha 1})k_{\alpha 1}\phi_1^r \tag{37}$$

They can again be expanded into a Fourier-Bessel series based on Lee and Cao (1989) and Todorovska and Lee (1991) if, taking Equation (33) for example,

$$P_{1t_{rr}}(r_1,\theta_1) = \frac{2\mu}{r_1^2}\sum_{n=0}^{+\infty}\left(A_{110,n}\cos n\theta_1 + B_{110,n}\sin n\theta_1\right) \tag{38}$$

where

$$A_{110,0} = \frac{r_1^2}{2\mu_s}\cdot\frac{a_n(r_1)}{2};\quad n = 0, N \tag{39}$$

$$A_{110,n} = \frac{r_1^2}{2\mu_s}a_n(r_1);\quad n = 1 \text{ to } (N-1) \tag{40}$$

and

$$B_{110,n} = \frac{r_1^2}{2u_s}b_n(r_1);\quad n = 0 \text{ to } N \tag{41}$$

and $a_n(r_1)$ and $b_n(r_1)$ can be estimated discretely by

$$a_n(r_1) = \frac{1}{N}\sum_{l=0}^{2N-1}P_{1t_{rr}}\left(r_1,\frac{\pi l}{N}\right)\cos\left(\frac{\pi l}{N}n\right);\quad n = 0 \text{ to } N \tag{42}$$

$$b_n(r_1) = \frac{1}{N}\sum_{l=0}^{2N-1}P_{1t_{rr}}\left(r_1,\frac{\pi l}{N}\right)\sin\left(\frac{\pi l}{N}n\right);\quad n = 0 \text{ to } N \tag{43}$$

In the same way, $P_{1t_{r\theta}}(r_1,\theta_1)$, $P_{1\sigma}(r_1,\theta_1)$, $P_{1u_r}(r_1,\theta_1)$, and $P_{1U_r}(r_1,\theta_1)$ can be expanded into

$$P_{1t_{r\theta}}(r_1,\theta_1)=\frac{2u}{r_1^2}\sum_{n=0}^{+\infty}\left(A_{120,n}\cos n\theta_1+B_{120,n}\sin n\theta_1\right) \tag{44}$$

$$P_{1\sigma}(r_1,\theta_1)=\frac{2u}{r_1^2}\sum_{n=0}^{+\infty}\left(A_{130,n}\cos n\theta_1+B_{130,n}\sin n\theta_1\right) \tag{45}$$

$$P_{1u_r}(r_1,\theta_1)=\frac{1}{r_1}\sum_{n=0}^{+\infty}\left(A_{140,n}\cos n\theta_1+B_{140,n}\sin n\theta_1\right) \tag{46}$$

$$P_{1U_r}(r_1,\theta_1)=\frac{1}{r_1}\sum_{n=0}^{+\infty}\left(A_{150,n}\cos n\theta_1+B_{150,n}\sin n\theta_1\right) \tag{47}$$

Case III and Case IV: These cases are for the incident angle less than the second critical angle ($\theta_\beta<\theta_{\mathrm{cr2}}$) and greater than or equal to the second critical angle ($\theta_\beta\geq\theta_{\mathrm{cr2}}$), and are similar to Case I and Case II, respectively. The details can be seen in Liang et al. (2006a) and will not be discussed here for the sake of brevity.

For convenience and simplicity, the large circular surface used in Lee and Cao (1989) and Lee and Karl (1992, 1993) is used here to simulate the surface of the half-space (see Figure 1). It can be shown that when the radius of the large circular surface *R* is large enough, the error due to the approximation is small and can be neglected. Here, the curved surface of the approximated half-space is concave downward, with the center of the large radius far below the canyon center. Alternately, the curved surface of the approximated half-space can also be concave upward, with the center of the large radius then being far above the canyon center. Davis et al. (2001) have successfully used this later model in their above-mentioned paper. As stated in the paper, their results are consistent and in agreement with the earlier results of Lee and Karl (1992, 1993) which uses the present model to solve the same problem as Davis et al. (2001) on the "diffraction of SV waves by underground, circular cylindrical cavities". Both models have also been used and analyzed in the present paper, and with a large enough radius both approaches give results that are consistent and in agreement with each other.

In the presence of the underground circular cavity, scattering waves are generated. In the half-space, there exist scattered $\mathrm{P_I}$ waves $\phi_{11}(r_1,\theta_1)$, $\mathrm{P_{II}}$ waves $\phi_{12}(r_1,\theta_1)$, SV waves $\psi_1(r_1,\theta_1)$ due to the cavity, and scattered $\mathrm{P_I}$ waves $\phi_{21}(r_2,\theta_2)$, $\mathrm{P_{II}}$ waves $\phi_{22}(r_2,\theta_2)$, and SV waves $\psi_2(r_2,\theta_2)$ due to the half-space surface (approximated here as an almost flat circular surface with a very large radius), and these waves are to be expressed as a Fourier-Bessel series with regard to their respective coordinate systems (r_1,θ_1) and (r_2,θ_2):

$$\phi_{11}(r_1,\theta_1)=\sum_{n=0}^{\infty}H_n^{(1)}(k_{\alpha1}r_1)\left(A_{\mathrm{s}11,n}^{(1)}\cos n\theta_1+B_{\mathrm{s}11,n}^{(1)}\sin n\theta_1\right) \tag{48}$$

$$\phi_{12}(r_1,\theta_1)=\sum_{n=0}^{\infty}H_n^{(1)}(k_{\alpha2}r_1)\left(A_{\mathrm{s}12,n}^{(1)}\cos n\theta_1+B_{\mathrm{s}12,n}^{(1)}\sin n\theta_1\right) \tag{49}$$

$$\psi_1(r_1,\theta_1)=\sum_{n=0}^{\infty}H_n^{(1)}(k_{\beta}r_1)\left(c_{\mathrm{s}1,n}^{(1)}\sin n\theta_1+D_{\mathrm{s}1,n}^{(1)}\cos n\theta_1\right) \tag{50}$$

$$\phi_{21}(r_2,\theta_2)=\sum_{m=0}^{\infty}J_m(k_{\alpha1}r_2)\left(A_{\mathrm{s}21,m}^{(2)}\cos m\theta_2+B_{\mathrm{s}21,m}^{(2)}\sin m\theta_2\right) \tag{51}$$

$$\phi_{22}(r_2,\theta_2)=\sum_{m=0}^{\infty}J_m(k_{\alpha2}r_2)\left(A_{\mathrm{s}22,m}^{(2)}\cos m\theta_2+B_{\mathrm{s}22,m}^{(2)}\sin m\theta_2\right) \tag{52}$$

$$\psi_2(r_2,\theta_2)=\sum_{m=0}^{\infty}J_m(k_{\beta}r_2)\left(c_{\mathrm{s}2,m}^{(2)}\sin m\theta_2+D_{\mathrm{s}2,m}^{(2)}\cos m\theta_2\right) \tag{53}$$

where, $J_m(.)$ and $H_n^{(1)}(.)$ are the Bessel function of the first kind and the Hankel function, respectively; $\phi_{11}(r_1,\theta_1)$, $\phi_{12}(r_1,\theta_1)$, and $\psi_1(r_1,\theta_1)$ are outgoing waves scattering away from the center O_1 of the cavity; and $\phi_{21}(r_2,\theta_2)$, $\phi_{22}(r_2,\theta_2)$, and $\psi_2(r_2,\theta_2)$ are standing waves resulting from the reflection of waves back and forth between the interface $r_1 = a$ and the curved surface of the half-space $r_2 = R$.

Therefore, the total resultant wave-potential functions in the half-space can be written as

$$\phi = \phi_1^{(r)} + \phi_2^{(r)} + \phi_{11} + \phi_{12} + \phi_{21} + \phi_{22} \tag{54}$$

$$\psi = \psi^{(i)} + \psi^{(r)} + \psi_1 + \psi_2 \tag{55}$$

3. Boundary Conditions and the Solution

The boundary conditions in our model for the drained case are

$$\begin{aligned} \tau_{rr} &= 0 \\ \tau_{r\theta} &= 0 \\ \sigma &= 0 \end{aligned} \tag{56}$$

at a large, circular, free-field surface of a half-space $(r_2 = R)$, and

$$\begin{aligned} \tau_{rr} &= 0 \\ \tau_{r\theta} &= 0 \\ \sigma &= 0 \end{aligned} \tag{57}$$

at the surface of the cavity $(r_1 = b)$. The boundary conditions for the undrained case are

$$\begin{aligned} \tau_{rr} + \sigma &= 0 \\ \tau_{r\theta} &= 0 \\ u_r - U_r &= 0 \end{aligned} \tag{58}$$

at a large, circular, free-field surface of a half-space $(r_2 = R)$, and

$$\begin{aligned} \tau_{rr} + \sigma &= 0 \\ \tau_{r\theta} &= 0 \\ u_r - U_r &= 0 \end{aligned} \tag{59}$$

at the surface of the cavity $(r_1 = b)$.

This plane-strain problem for the incident SV waves is very similar to that of the incident SV waves on a semi-circular canyon in a poroelastic half-space (Liang et al., 2006a, 2006b). Much of the formulae and derivations are identical and will not be repeated here. The displacements and stresses can thus be expressed as

$$\tau_{rr} = \sum_{j=1}^{2}\left[\left(\lambda + f_j Q\right)\nabla^2\phi_j + 2\mu\frac{\partial^2\phi_j}{\partial r^2}\right] + 2\mu\frac{\partial}{\partial r}\left[\frac{1}{r}\frac{\partial\psi}{\partial\theta}\right] \tag{60}$$

$$\tau_{r\theta} = \sum_{j=1}^{2}\left[2\mu\left(\frac{1}{r}\frac{\partial^2\phi_j}{\partial r\partial\theta} - \frac{1}{r^2}\frac{\partial\phi_j}{\partial\theta}\right)\right] + \mu\left[\frac{1}{r^2}\frac{\partial^2\psi}{\partial\theta^2} - r\frac{\partial}{\partial r}\left(\frac{1}{r}\frac{\partial\psi}{\partial r}\right)\right] \tag{61}$$

$$\sigma = \sum_{j=1}^{2}\left(Q + f_j R\right)\nabla^2\phi_j \tag{62}$$

$$u_r = \sum_{j=1}^{2}\frac{\partial\phi_j}{\partial r} + \frac{1}{r}\frac{\partial\psi}{\partial\theta} \tag{63}$$

$$u_\theta = \sum_{j=1}^{2} \frac{1}{r}\frac{\partial \phi_j}{\partial \theta} - \frac{\partial \psi}{\partial r} \tag{64}$$

$$U_r = \sum_{j=1}^{2} f_j \frac{\partial \phi_j}{\partial r} + f_3 \frac{1}{r}\frac{\partial \psi}{\partial \theta} \tag{65}$$

$$U_\theta = \sum_{j=1}^{2} f_j \frac{1}{r}\frac{\partial \phi_j}{\partial \theta} - f_3 \frac{\partial \psi}{\partial r} \tag{66}$$

By introducing the boundary conditions, all of the coefficients of Equations. (48)–(53) can be solved, and the solution can be used to calculate the surface displacement near the cavity through Equations (54), (55), (63), and (64).

VERIFICATION OF ACCURACY OF THE SOLUTION

The accuracy of the solution depends upon the truncation of the infinite series and can be checked by the extent to which it satisfies the boundary conditions. A dimensionless frequency parameter is defined as

$$\eta = 2a / \lambda_\beta \tag{67}$$

where λ_β is the wavelength of the incident waves in the half-space. We further define the residuals as

$$\tau_{rr}^{*} = \tau_{rr} / \sigma_0 \tag{68}$$

$$\tau_{r\theta}^{*} = \tau_{r\theta} / \sigma_0 \tag{69}$$

$$\sigma^{*} = \sigma / \sigma_0 \tag{70}$$

for the case of the drained boundary condition, and the residuals

$$(\tau_{rr} + \sigma)^{*} = (\tau_{rr} + \sigma) / \sigma_0 \tag{71}$$

$$\tau_{r\theta}^{*} = \tau_{r\theta} / \sigma_0 \tag{72}$$

$$(u_r - U_r)^{*} = (u_r - U_r) / u_0 \tag{73}$$

for the case of the undrained boundary condition, where σ_0 and u_0 are the stress intensity and displacement intensity, respectively, of the incident waves.

Figures 2(a) and 2(b) show the convergence of averaged residuals (over the range of $\theta_1 = -180°$ to 180° with the interval of 1°) at the boundary $r_1 = a$ with the truncation order N at $\theta_\beta = 30°$ for porosity n = 0.3; Poisson's ratio ν = 0.25; dimensionless frequencies η = 1.0, 3.0, and 5.0; and the drained boundary and undrained boundary, respectively. Figures 3(a) and 3(b) illustrate the boundary residuals at truncation orders N = 25, 40, and 50 and dimensionless frequencies η = 1.0, 3.0, and 5.0, for the drained boundary and undrained boundary, respectively. It is shown that the averaged residuals decrease rapidly when the truncation order N increases; therefore, if the truncation order N is large enough, the boundary residuals can become small enough—i.e., the results would converge to the true solution. Further, as the incident frequency increases, large N is needed for a prescribed precision.

NUMERICAL RESULTS AND ANALYSIS

The material properties for the half-space were chosen for numerical examples with parameters, n_{cr} = 0.36, K_{cr} = 200 MPa, K_g = 36000 MPa, K_f = 2000 MPa, ρ_g = 2650 kg/m^3, and ρ_f = 1000 kg/m^3 (Lin et al., 2005). Four different porosities (n = 0.1, 0.3, 0.34, and 0.36), which correspond to the dry-frame bulk moduli (K_{dry}) of 26055, 6167, 2189, and 200 MPa, respectively, are used to evaluate the surface displacement amplitudes, and three different Poisson's ratios (ν = 0.2, 0.3, and 0.4) are used for

the comparison. Figure 4 illustrates the variations of velocities $c_{\alpha 1}$, $c_{\alpha 2}$, and c_{β}, respectively, versus porosity and Poisson's ratio.

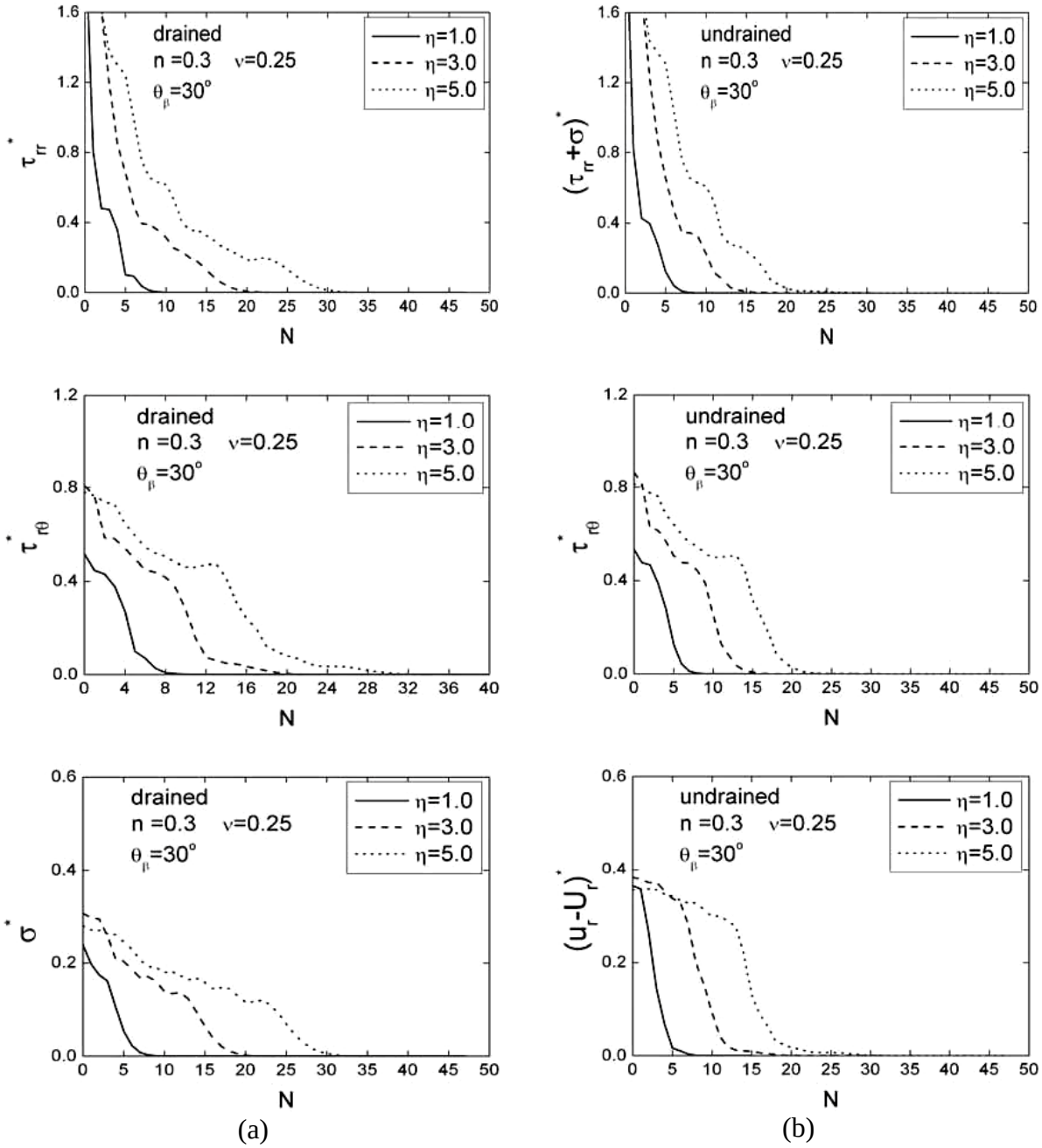

Fig. 2 Convergence of averaged residuals at the boundary $r_1 = a$ as the truncation order N increases: (a) Drained boundary; (b) Undrained boundary

Figures 5–7 show the horizontal (X) and vertical (Y) surface displacement amplitudes near the cavity in a drained saturated poroelastic half-space, an undrained saturated poroelastic half-space, and a dry poroelastic half-space, respectively, with porosity n = 0.3, Poisson's ratio ν = 0.25, and dimensionless frequencies η of 1.0, 3.0, and 5.0. The surface displacement amplitudes are normalized by the displacement intensity of the incident SV waves. It should be noted that all of the surface displacements refer to the half-space in this paper. The surface displacement amplitudes for the case of a dry poroelastic half-space for η = 1.0 (see Figure 5) are identical to those in Lee and Karl (1992). From these figures, it can be seen that the surface displacement amplitudes of the undrained saturated poroelastic medium are close to those of the drained saturated poroelastic medium; however, depending upon the incident angle, the surface displacement amplitudes of the dry poroelastic medium and of the saturated poroelastic media

(either drained or undrained) may be very different. For example, when the incident angle θ_β in Figures 5–7 is 30°, a large amplitude difference and phase shift can be observed, as well as a slight increase in the resultant wavelengths for the saturated cases, which can be demonstrated further by the following example case. We also find that the difference between the surface displacement amplitudes of the drained and undrained saturated poroelastic media becomes larger as the incident frequency increases, which implies that drainage condition plays a more important role under the condition of higher frequencies. The wavelengths of the waves in the undrained saturated poroelastic medium are slightly longer than those of the drained saturated poroelastic medium. For nearly grazing incident waves, a standing wave pattern is observed for $x/a < -1$, which is similar to what happens near a canyon (Liang et al., 2006a, 2006b).

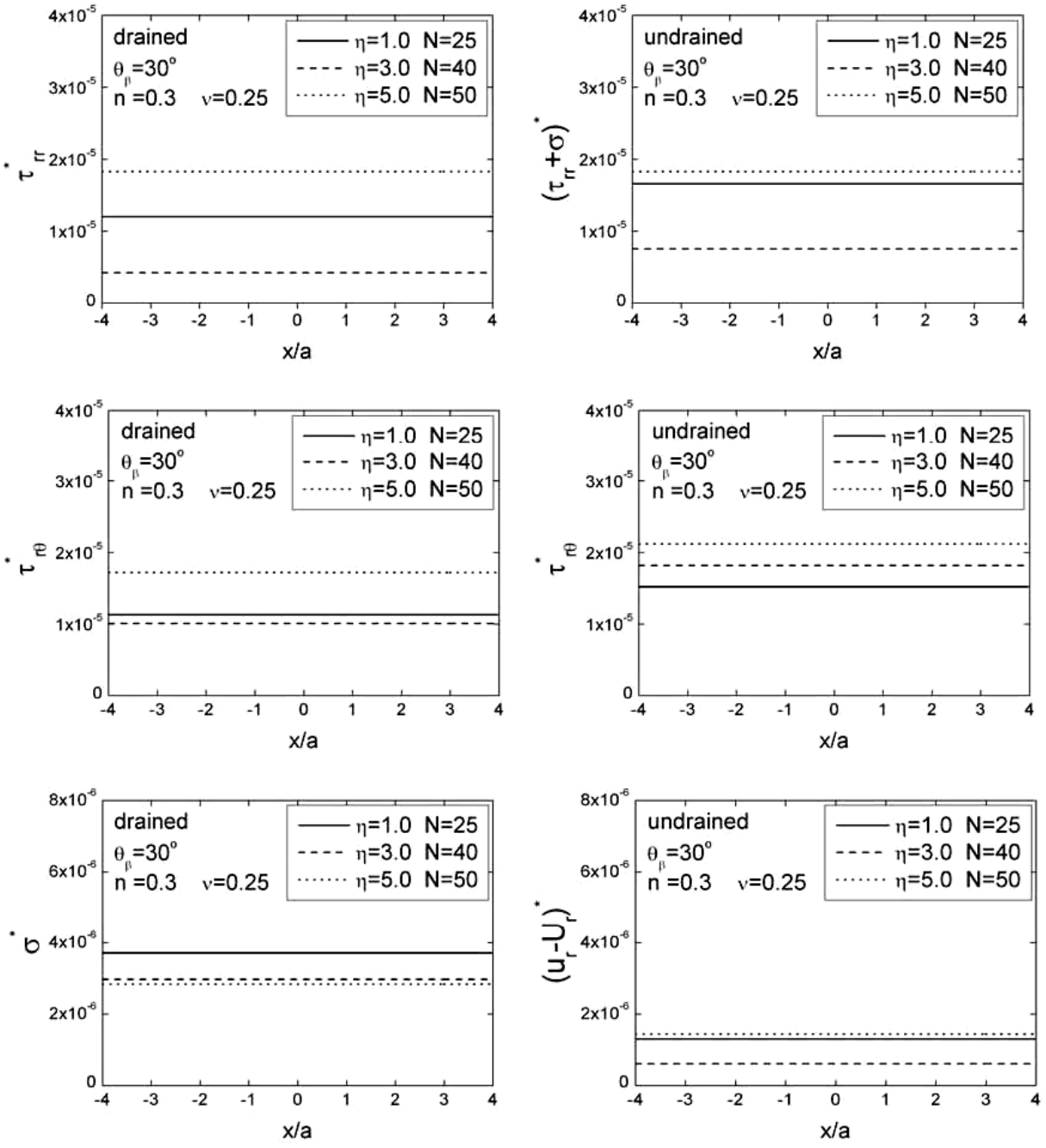

Fig. 3 Boundary residuals for specified truncation order N: (a) Drained boundary; (b) Undrained boundary

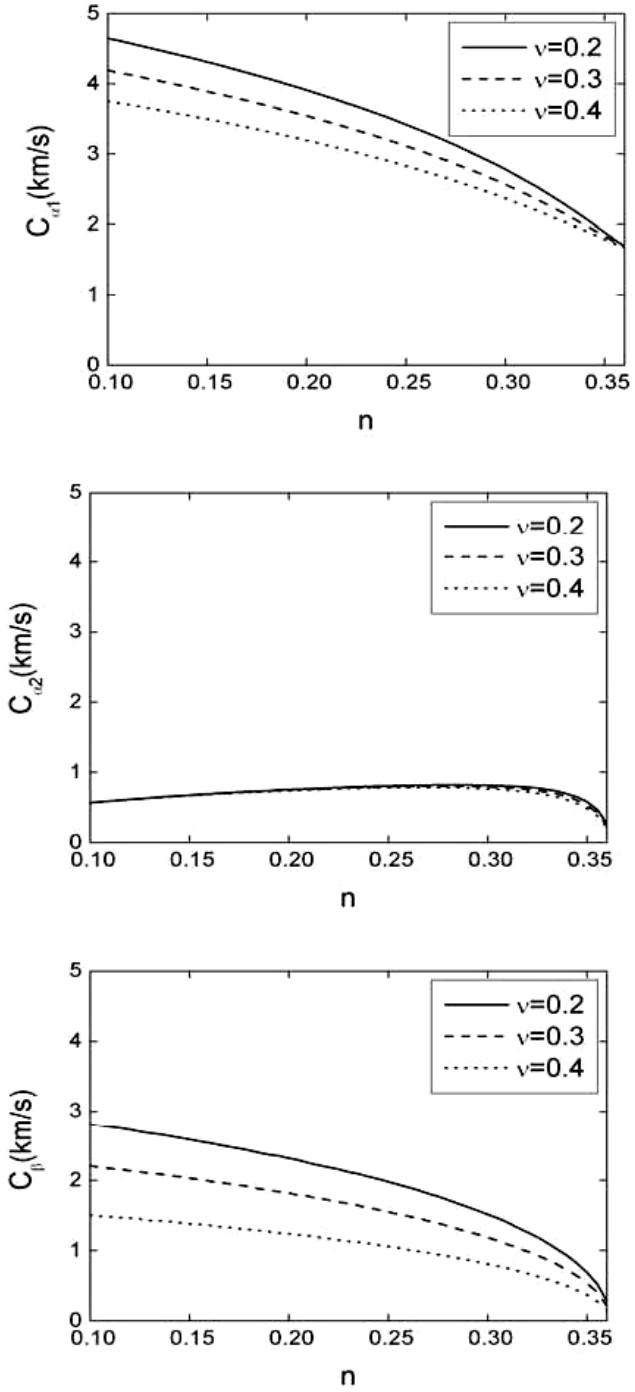

Fig. 4 Variation of velocities $c_{\alpha 1}$, $c_{\alpha 2}$ and c_{β} versus porosity n and Poisson's ratio ν

Figures 8 to 10 illustrate the surface displacement amplitudes at $x/a = -1, 0, 1$ versus incident angles for a drained saturated poroelastic half-space, an undrained saturated poroelastic half-space, and a dry poroelastic half-space, respectively, and for porosity $n = 0.25$, Poisson's ratio $\nu = 0.25$, and dimensionless frequencies $\eta = 1.0$, 3.0, and 5.0. The critical angles for the saturated poroelastic media and the dry poroelastic medium are 30.48° and 35.26°, respectively, which are both near the incident angle 30°. The two critical angles are not the same, and therefore, the surface displacement amplitudes for $\theta_{\beta} = 30°$ are very different, with the horizontal surface displacement amplitudes of the saturated poroelastic media being larger than those of the dry poroelastic medium. In contrast, at other incident angles—e.g., $\theta_{\beta} = 0°$, 60°, and 85° in Figures 5 to 7—there is not much difference between the surface displacement amplitudes of the saturated poroelastic media (either drained or undrained) and the dry poroelastic medium. As the incident frequency increases, the difference between the surface displacement amplitudes of the drained and undrained media becomes larger.

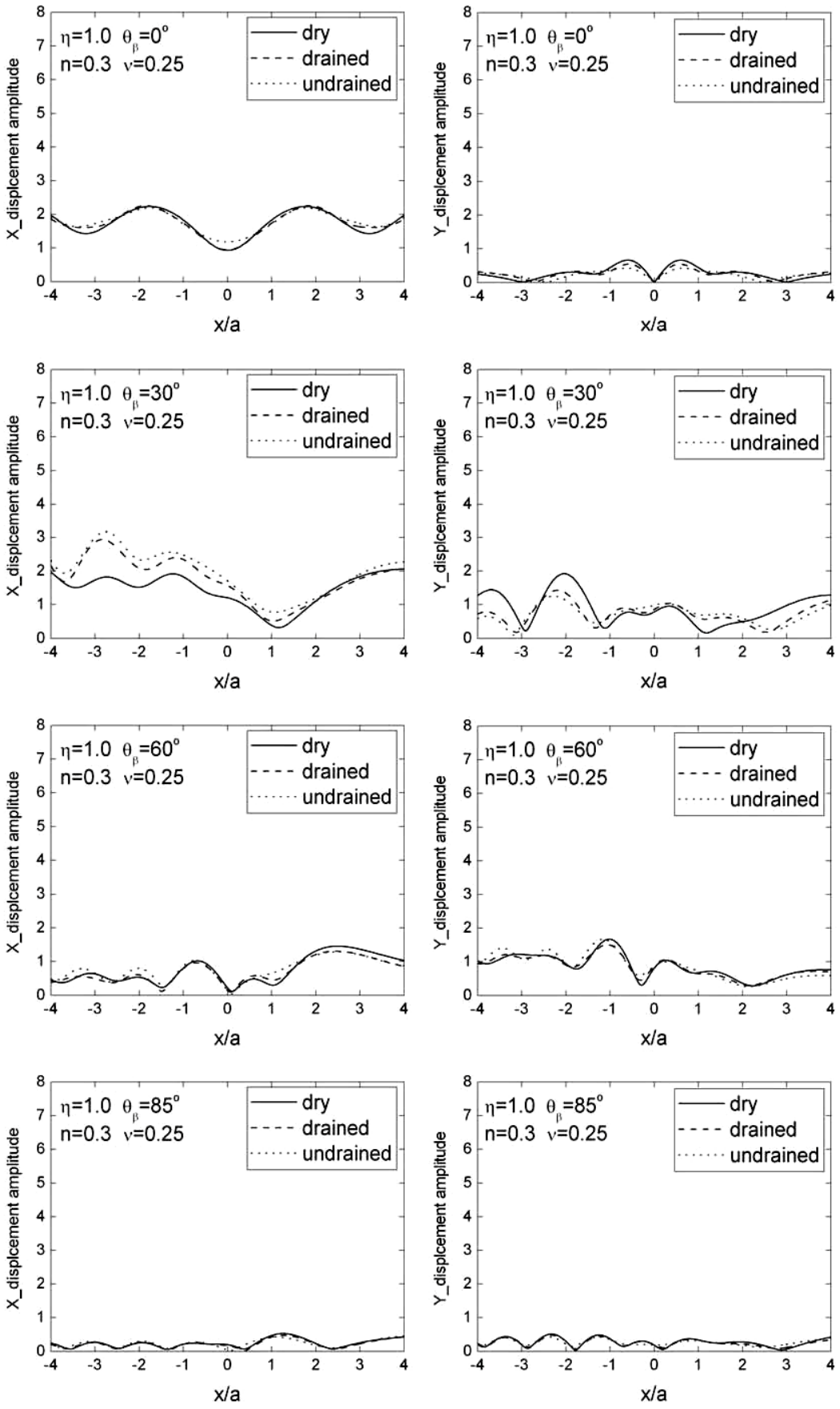

Fig. 5 Comparison between dry poroelastic, drained saturated poroelastic, and undrained saturated poroelastic half-spaces (η = 1.0)

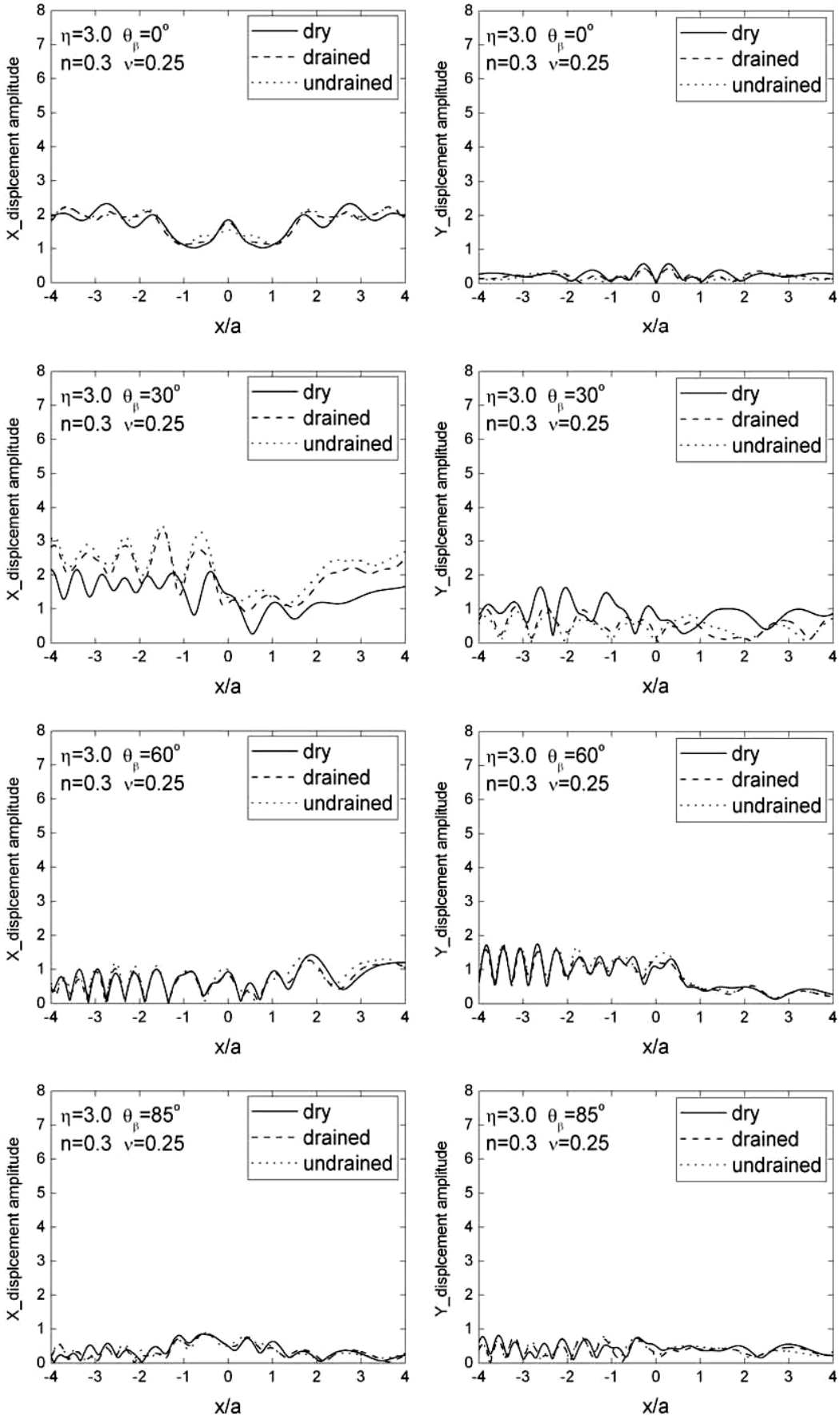

Fig. 6 Comparison between dry poroelastic, drained saturated poroelastic, and undrained saturated poroelastic half-spaces (η = 3.0)

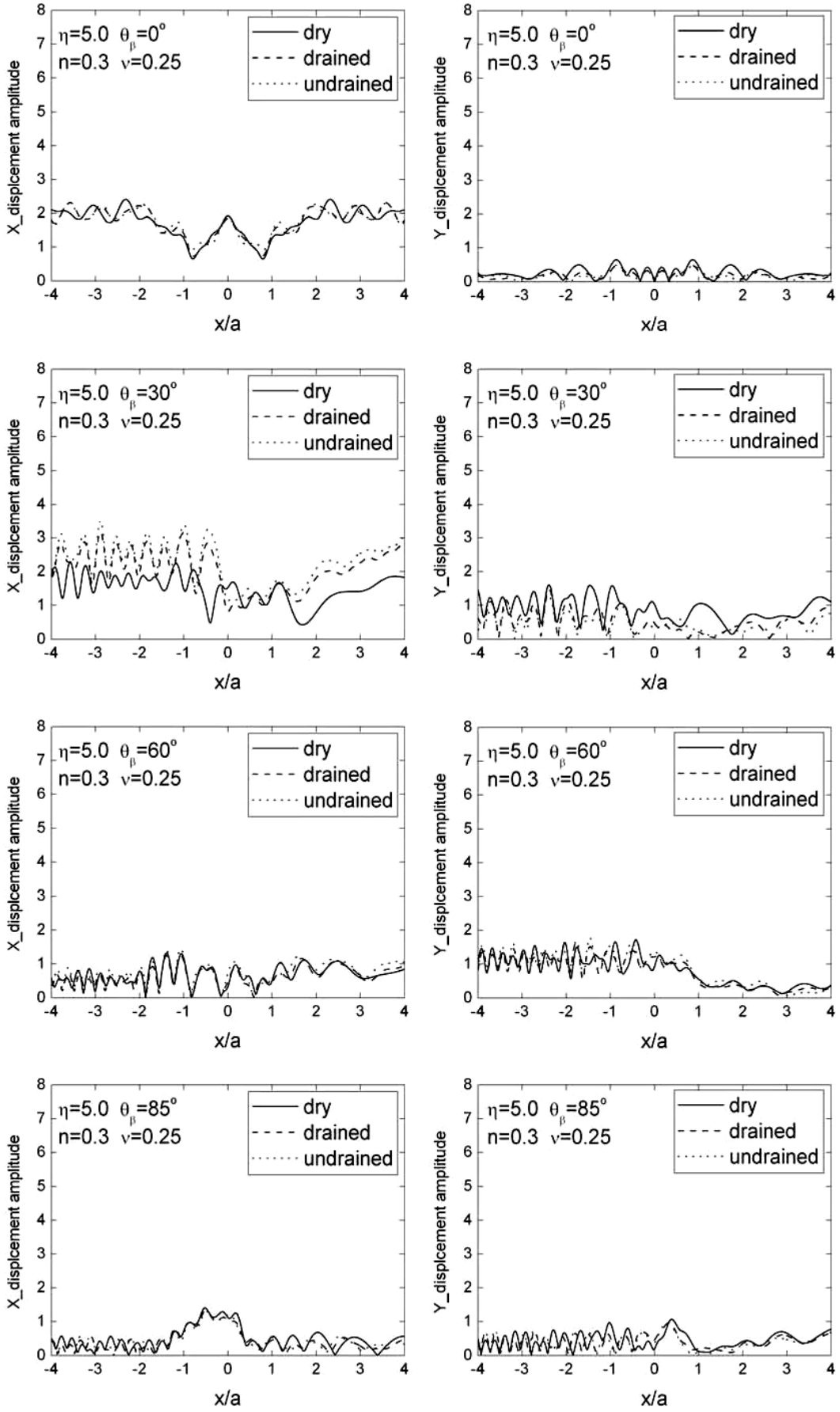

Fig. 7 Comparison between dry poroelastic, drained saturated poroelastic, and undrained saturated poroelastic half-spaces ($\eta = 5.0$)

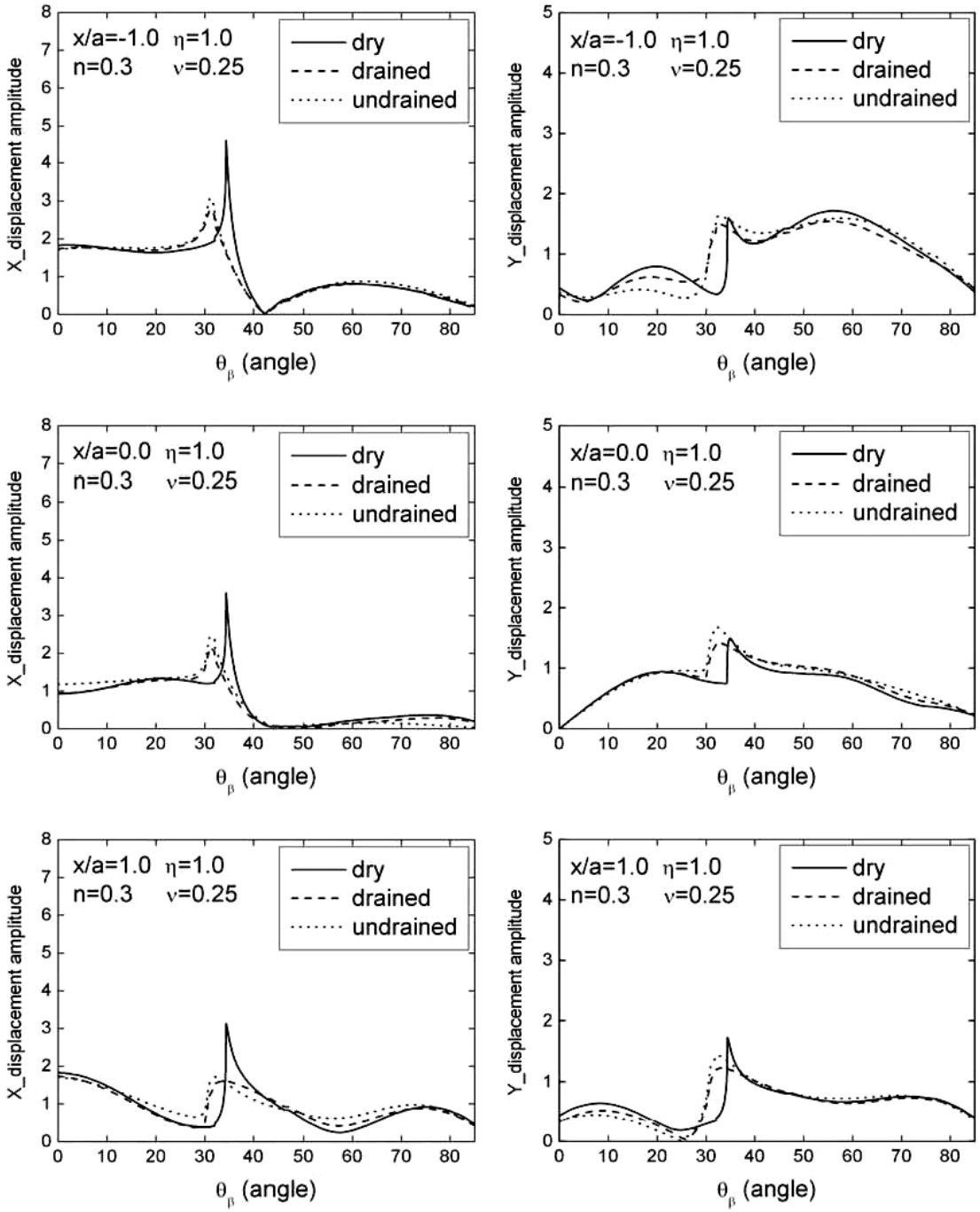

Fig. 8 Surface displacement at $x/a = -1$, 0, 1 versus incident angle for dry poroelastic, drained saturated poroelastic, and undrained saturated poroelastic half-spaces ($\eta = 1.0$)

Figures 11 to 14 illustrate the effects of porosity (n = 0.1, 0.3, 0.34, and 0.36) on the surface displacement amplitudes near the cavity in a saturated half-space for Poisson's ratio $\nu = 0.25$, incident angles $\theta_\beta = 30°$ and 60°, and dimensionless frequencies $\eta = 1.0$, 3.0, and 5.0. It can be seen that for small porosity (e.g., $n = 0.1$) the surface displacement amplitudes of the saturated poroelastic media (either drained or undrained) are almost identical to those of the dry poroelastic medium (see Figure 5 to 7), and drainage condition has little influence on the surface displacement amplitudes; while for large porosity (e.g., $n = 0.3$), the effect of drainage condition becomes significant. It can also be seen that, for the same porosity, the displacement amplitudes of the undrained saturated medium (see Figures 13 and 14) are larger than those in the drained saturated medium (see Figures 11 and 12). It should also be noted that the horizontal surface displacement amplitudes for porosity $n = 0.3$ and incident angle $\theta_\beta = 30°$ (see Figures 11 and 13) are larger than those for the other porosities, e.g., n = 0.1, 0.34 and 0.36, since the critical angle for the porosity $n = 0.3$ is nearest to the incident angle.

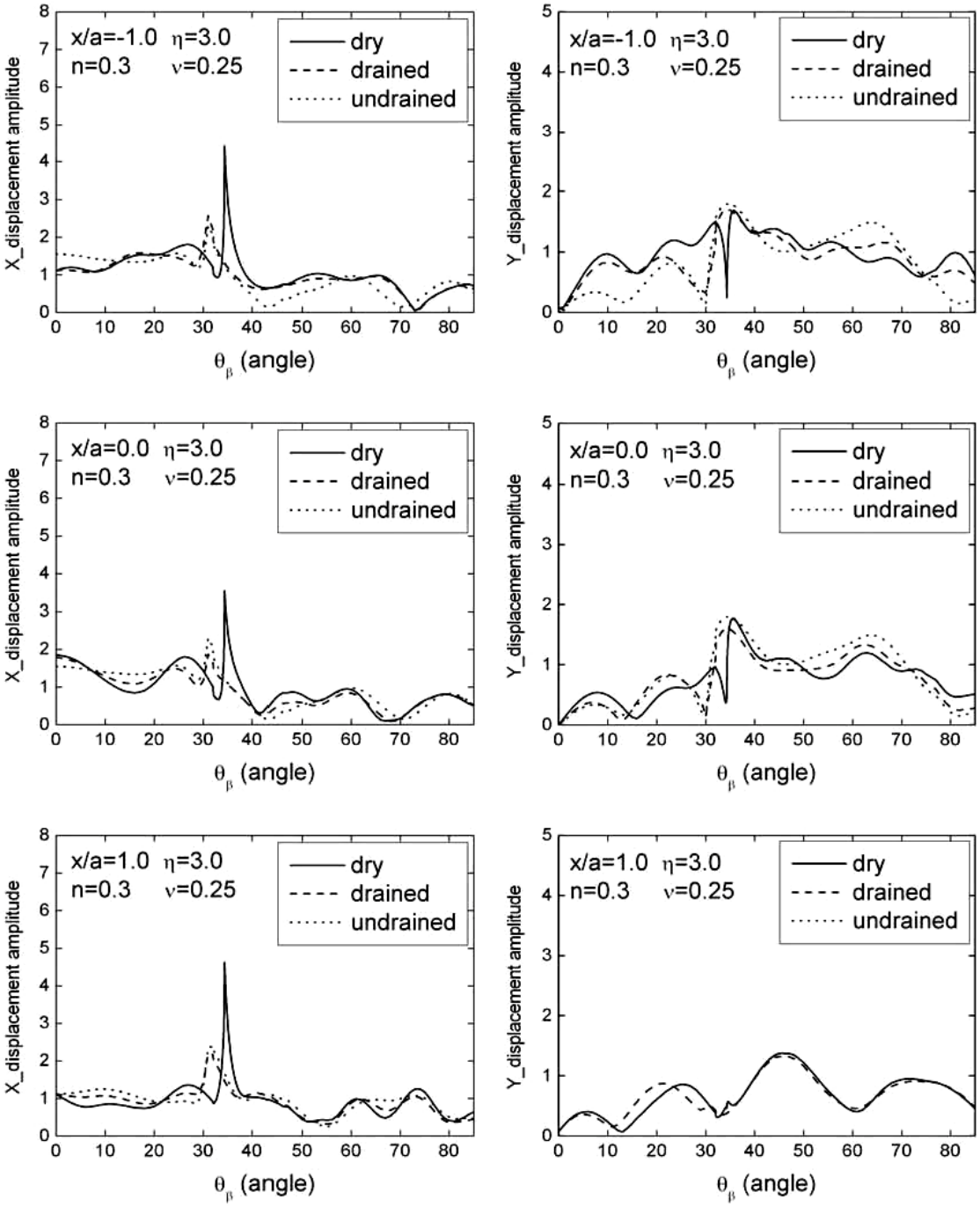

Fig. 9 Surface displacement at x/a = –1, 0, 1 versus incident angle for dry poroelastic, drained saturated poroelastic, and undrained saturated poroelastic half-spaces (η = 3.0)

Figures 15 to 18 illustrate the effects of Poisson's ratio (ν = 0.2, 0.3 and 0.4) on the surface displacement amplitudes near the cavity in a saturated half-space for porosity n = 0.3, incident angles θ_β = 30° and 60°, and dimensionless frequencies η = 1.0, 3.0 and 5.0, respectively. The critical angles of incidence for three Poisson's ratios, ν = 0.2, 0.3 and 0.4, are 33°, 27.58° and 19.98°, respectively. It can be seen from these figures that the horizontal surface displacement amplitudes for different Poisson's ratios are very different as, for example, for the incident angle θ_β = 30° large amplitude difference and phase shift are observed, and there is not much difference in the surface displacement amplitudes for the incident angle θ_β = 60°. This may be explained by noting that the incident angle θ_β = 30° is closer to the critical angle than θ_β = 60°. It can also be observed that Poisson's ratio has greater effect on the surface displacement amplitudes for the undrained saturated medium than for the drained saturated medium.

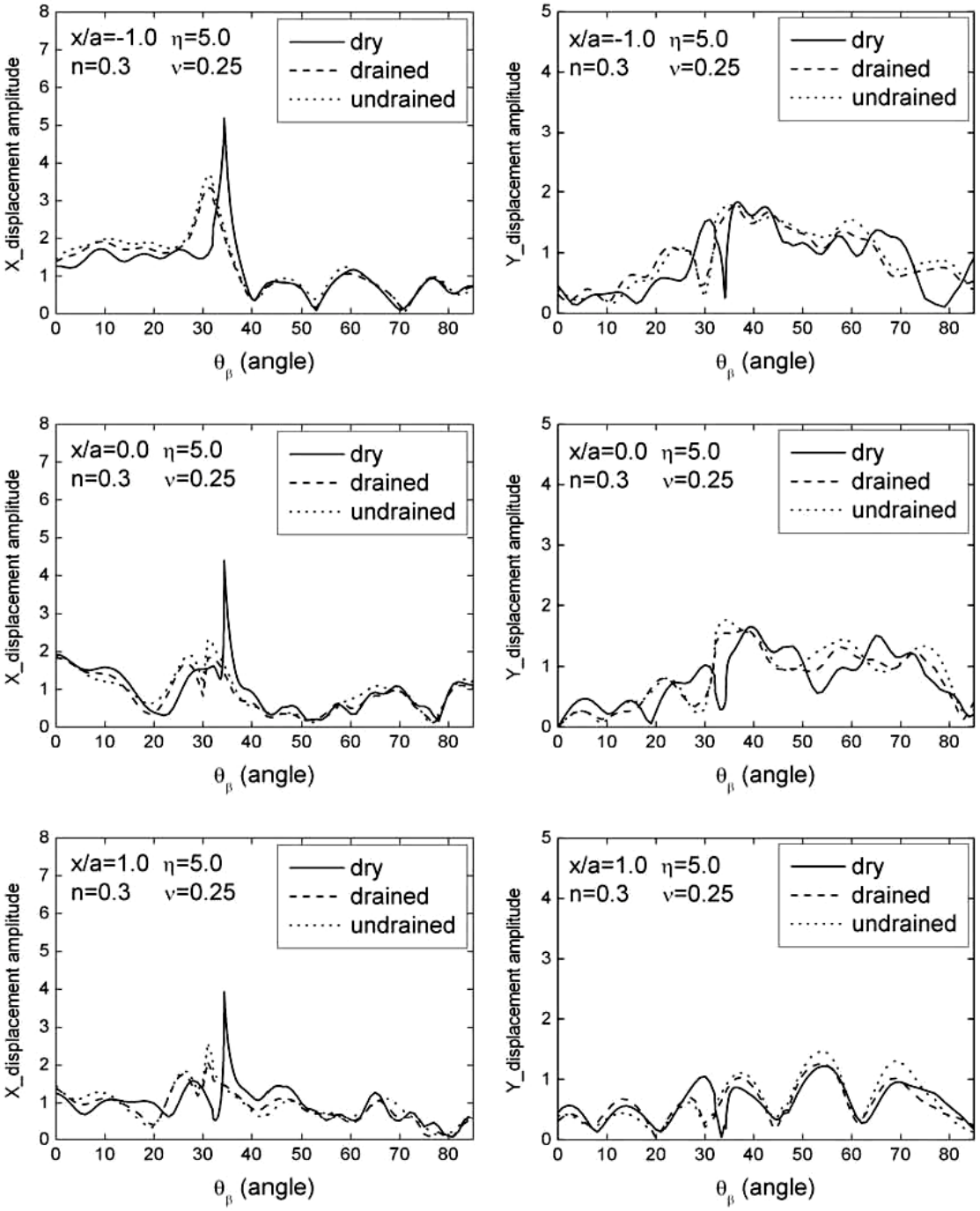

Fig. 10 Surface displacement at $x/a = -1, 0, 1$ versus incident angle for dry poroelastic, drained saturated poroelastic, and undrained saturated poroelastic half-spaces ($\eta = 5.0$)

Figures 19–22 and 23–26, respectively, illustrate the pore pressures along the surfaces of the half-space and the cavity, for porosities $n = 0.1$, 0.3, 0.34 and 0.36, with dimensionless frequencies $\eta = 1.0$, 3.0 and 5.0. The pore pressures are normalized by the stress amplitudes of the incident SV waves. It is seen that large pore pressures occur near or around the cavity, and that the pore pressures depend strongly on the incident angles, which may be due to the wave interference between the surface of the half-space and the cavity. As the porosity increases, the pore pressures increase significantly but their oscillations become smoother, which implies that more energy is taken by the pore fluid and less by the softer dry frame. Saturated poroelastic medium with larger porosities and more pore fluid (for larger pore sizes) will lead to smoother variation of pore pressures. As the dimensionless frequency increases, the pore pressures become more complicated, which suggests that the higher frequency waves may more easily stimulate pore pressures of large amplitudes and rapid fluctuations.

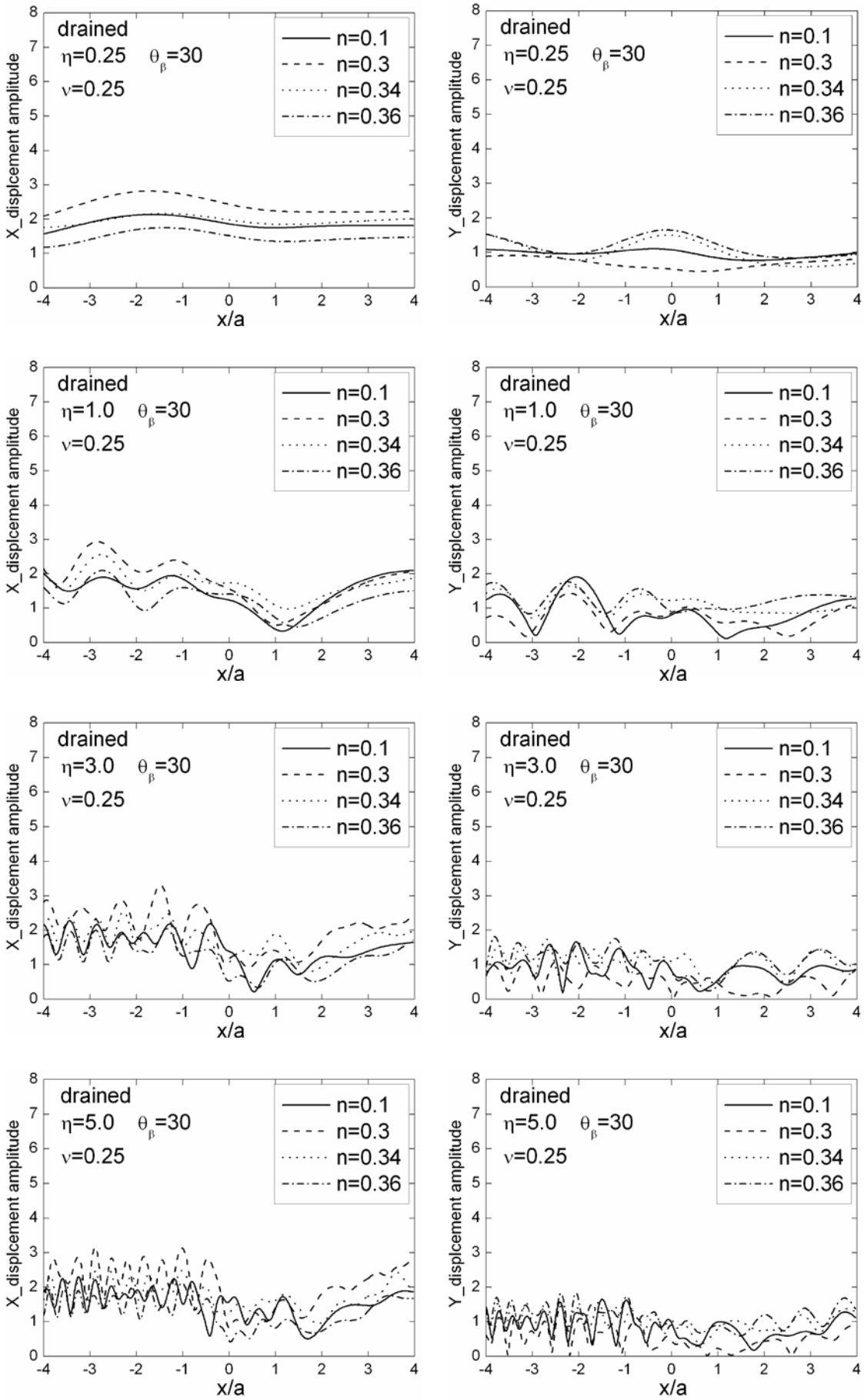

Fig. 11 Surface displacement versus porosity for drained boundary (θ_β = 30°)

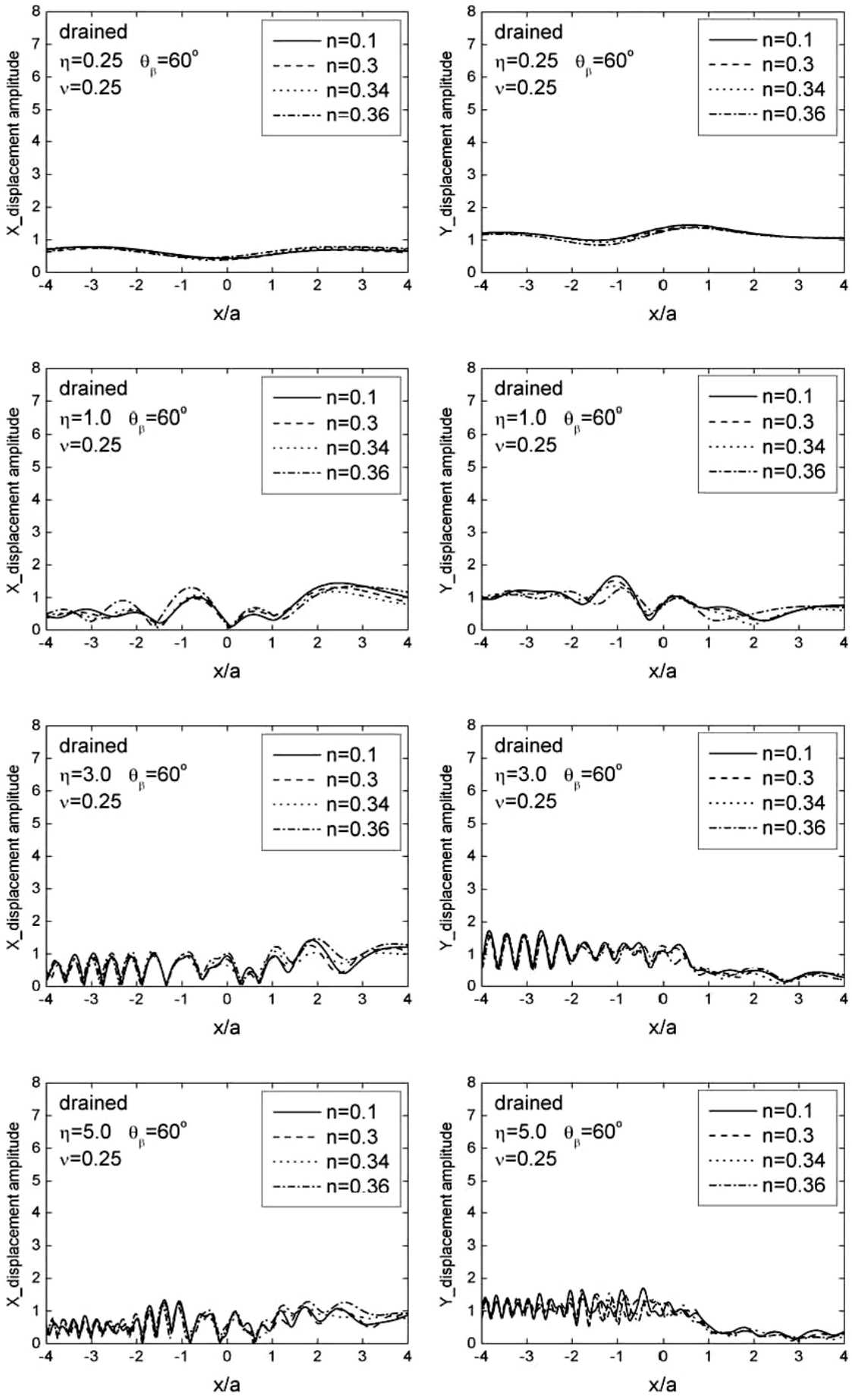

Fig. 12 Surface displacement versus porosity for drained boundary (θ_β = 60°)

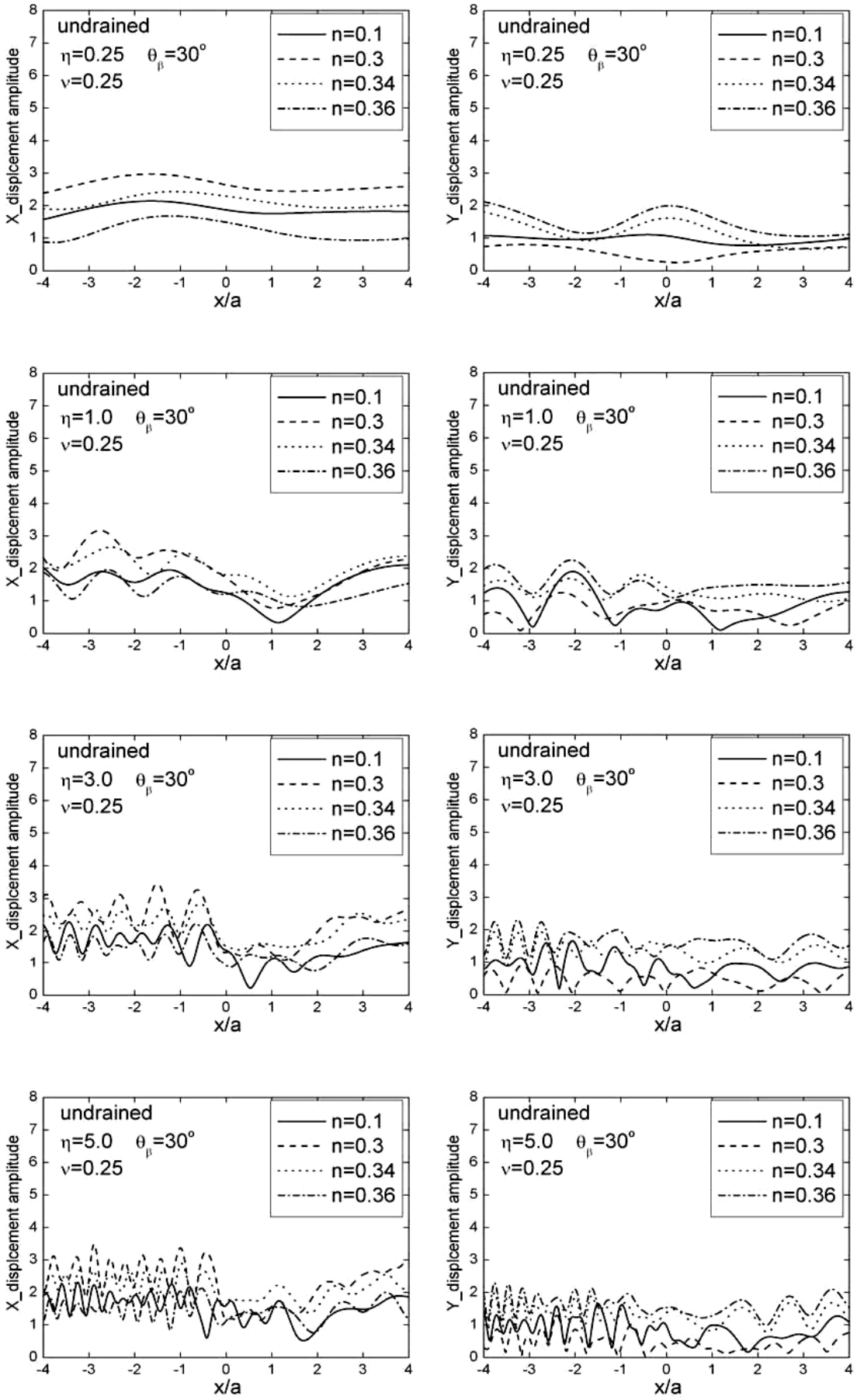

Fig. 13 Surface displacement versus porosity for undrained boundary (θ_β = 30°)

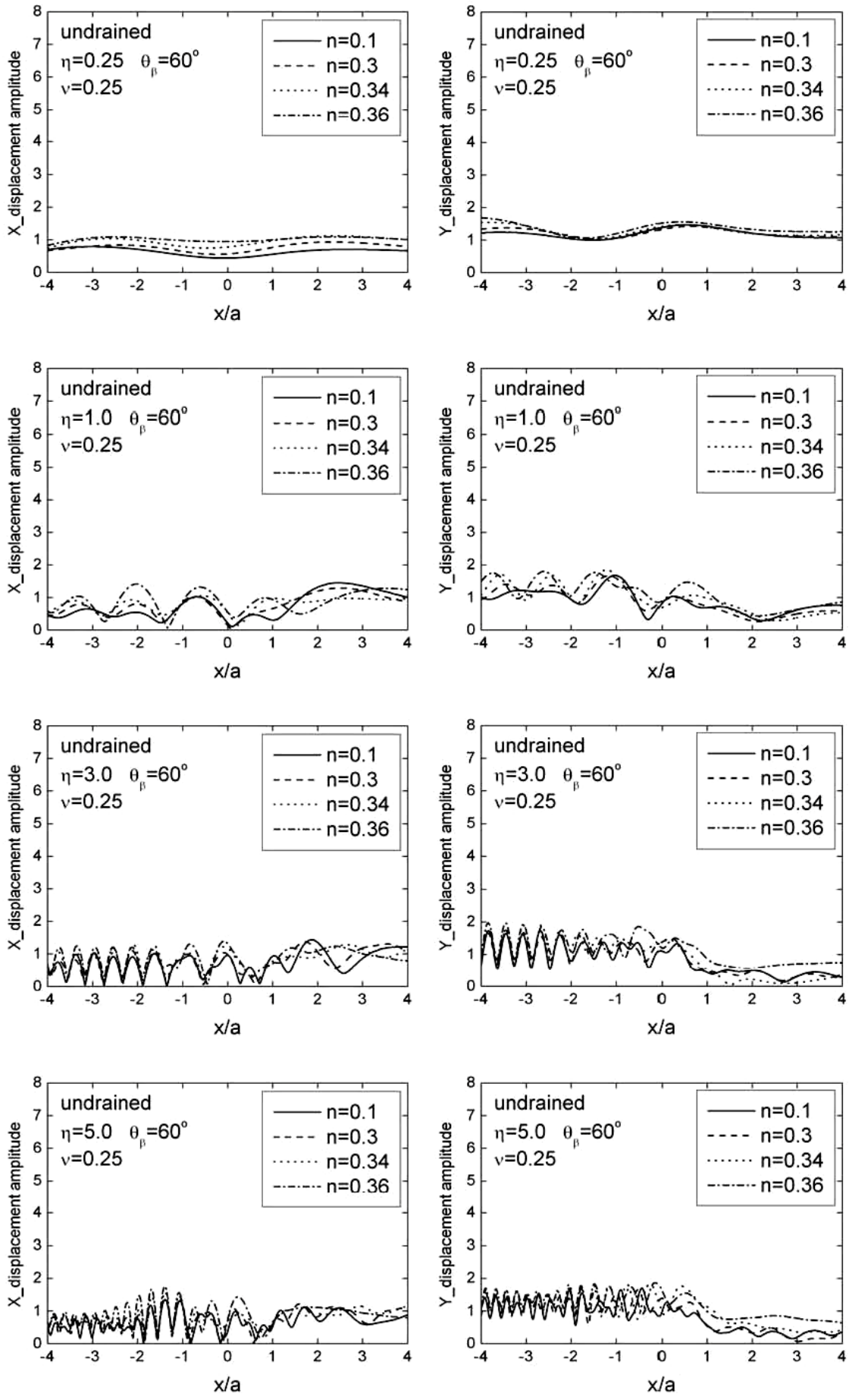

Fig. 14 Surface displacement versus porosity for undrained boundary (θ_β = 60°)

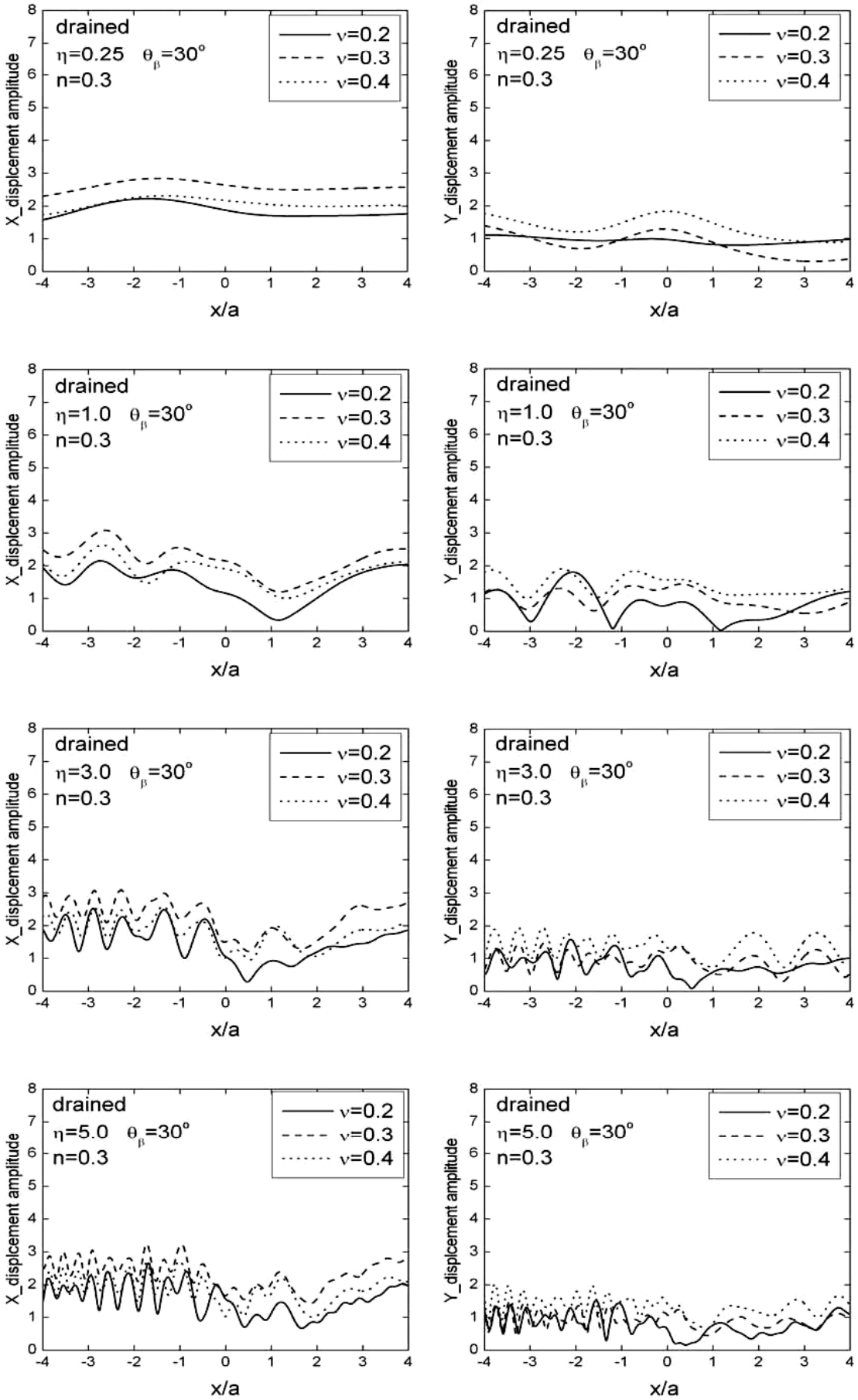

Fig. 15 Surface displacement versus Poisson's ratio for drained boundary (θ_β = 30°)

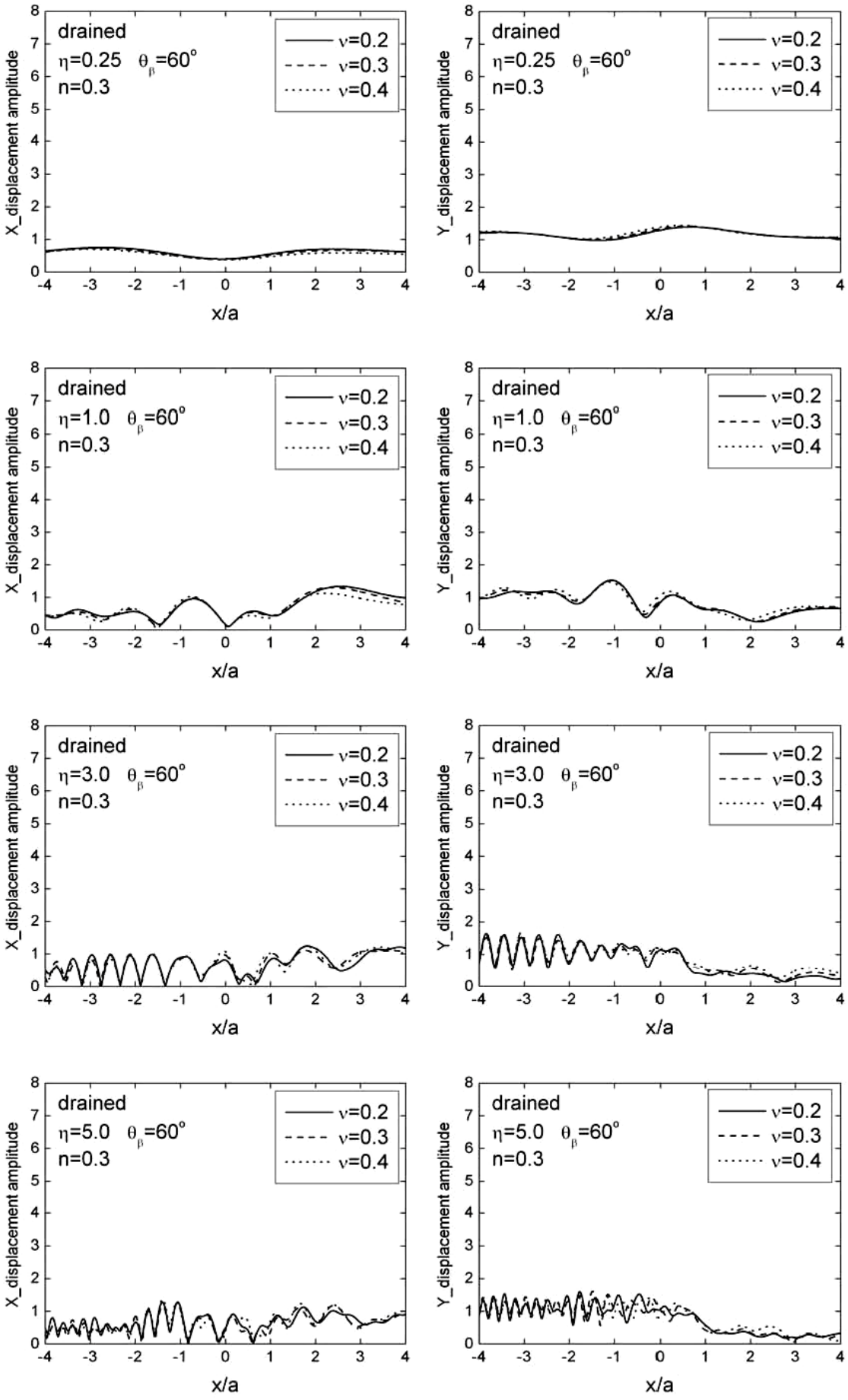

Fig. 16 Surface displacement versus Poisson's ratio for drained boundary (θ_β = 60°)

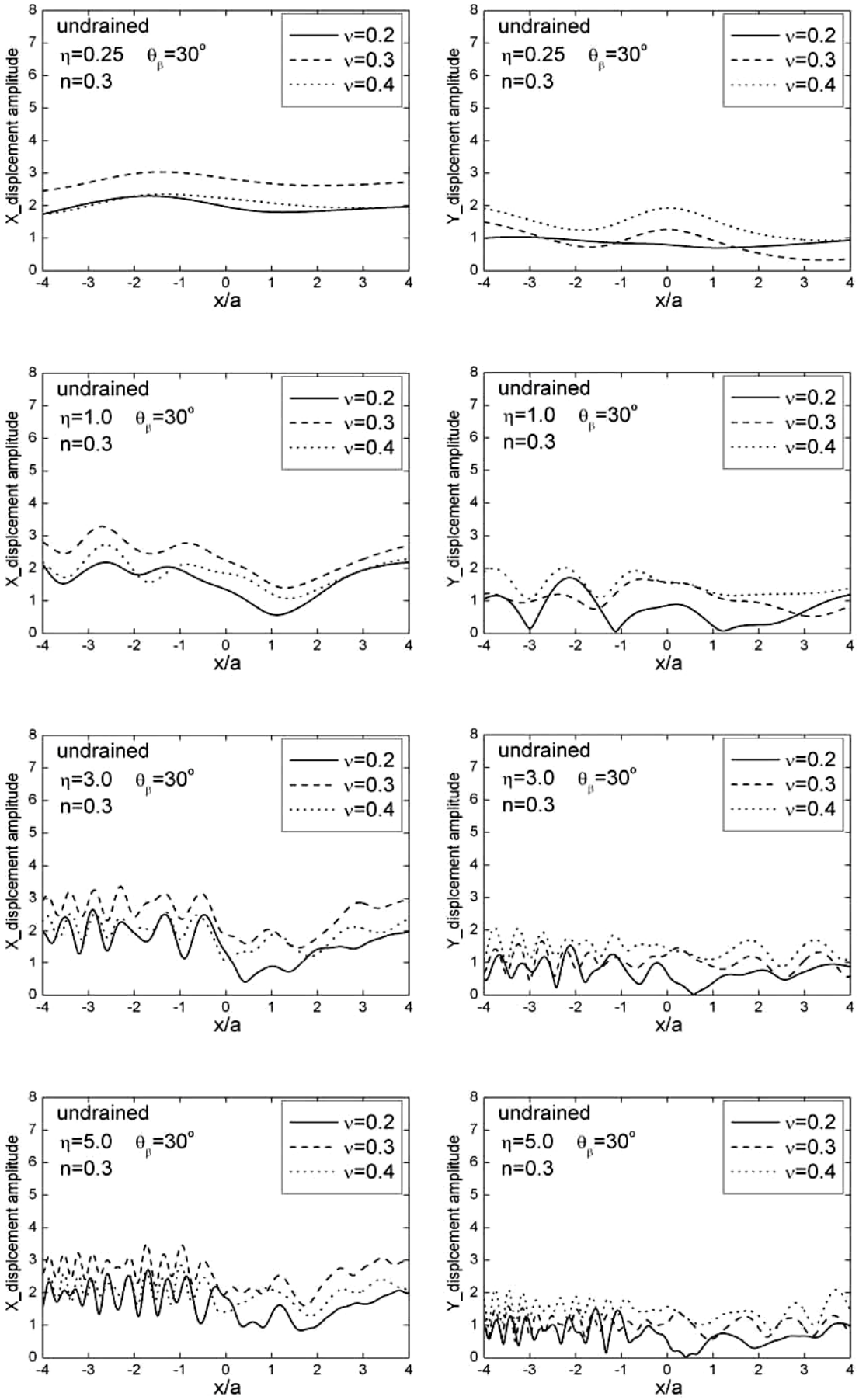

Fig. 17 Surface displacement versus Poisson's ratio for undrained boundary (θ_β = 30°)

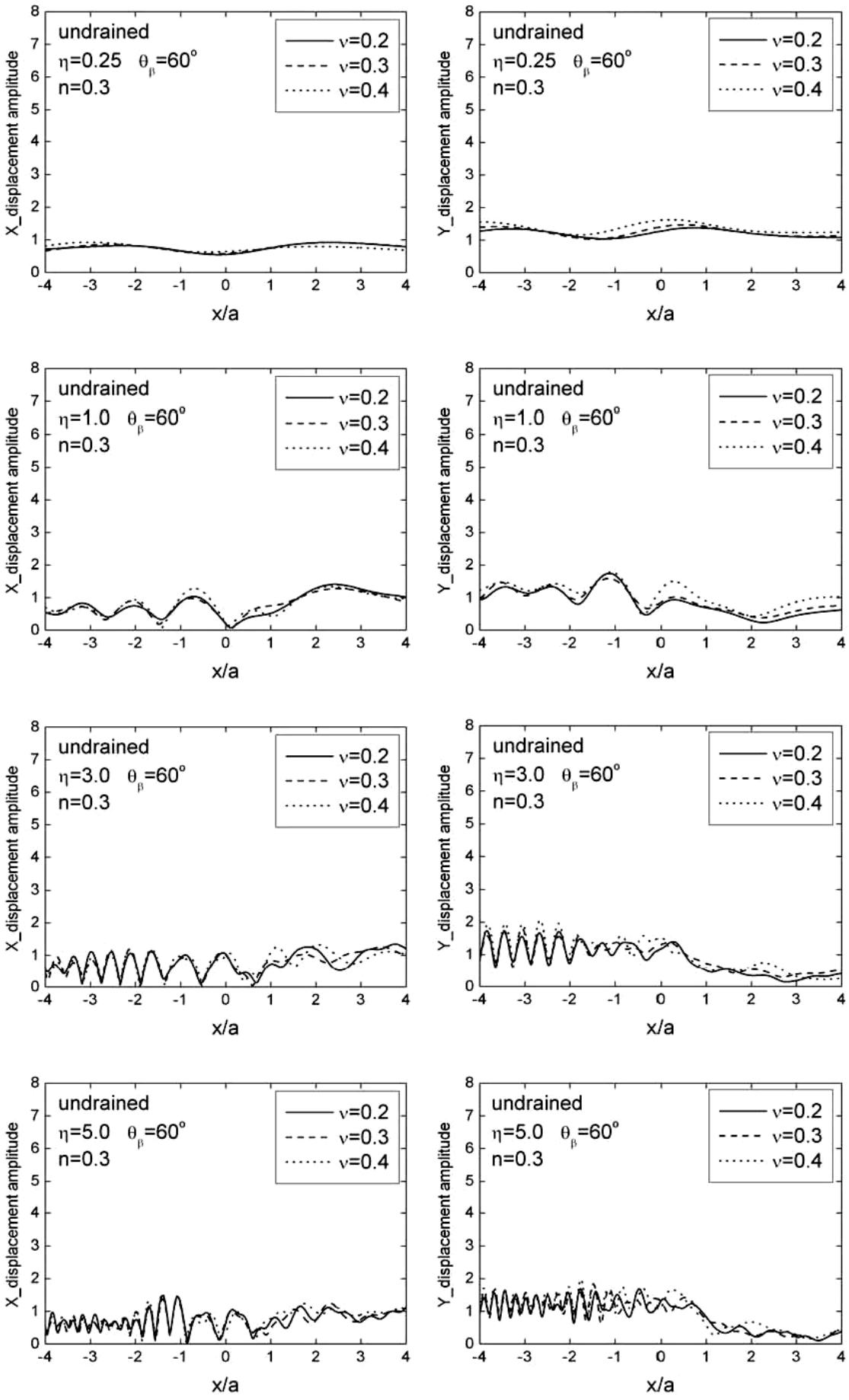

Fig. 18 Surface displacement versus Poisson's ratio for undrained boundary (θ_β = 60°)

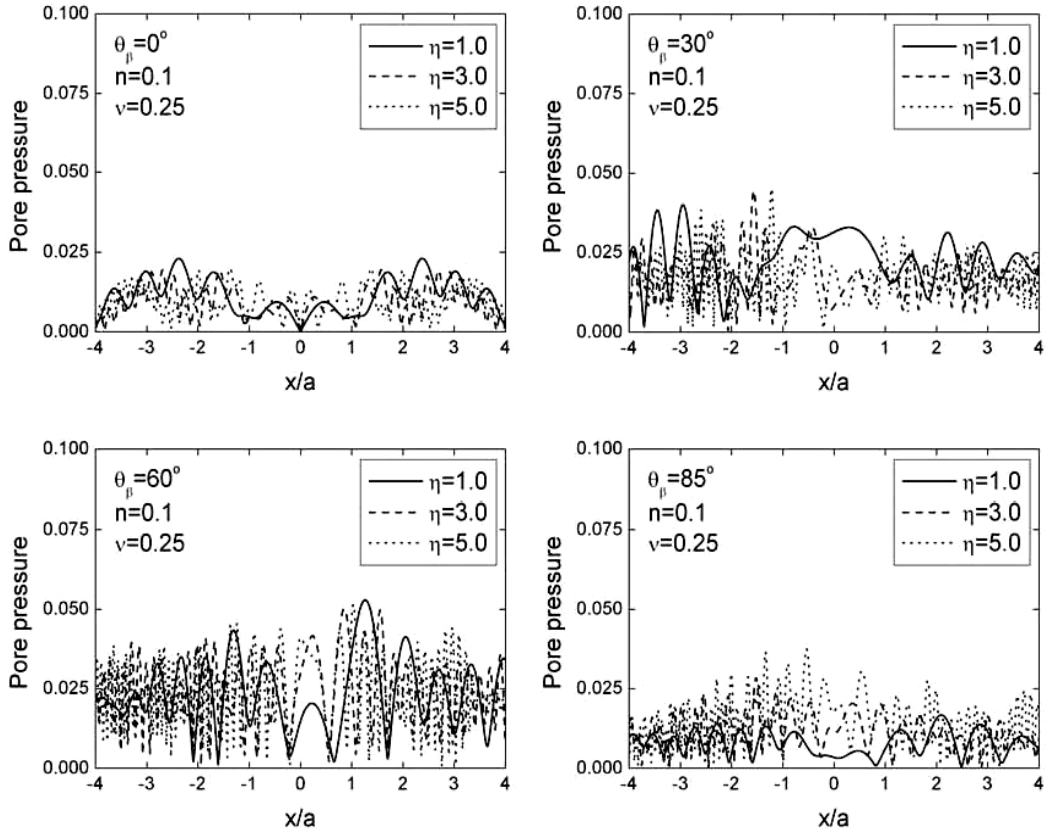

Fig. 19 Pore pressure along surface of half-space versus porosity (n = 0.1)

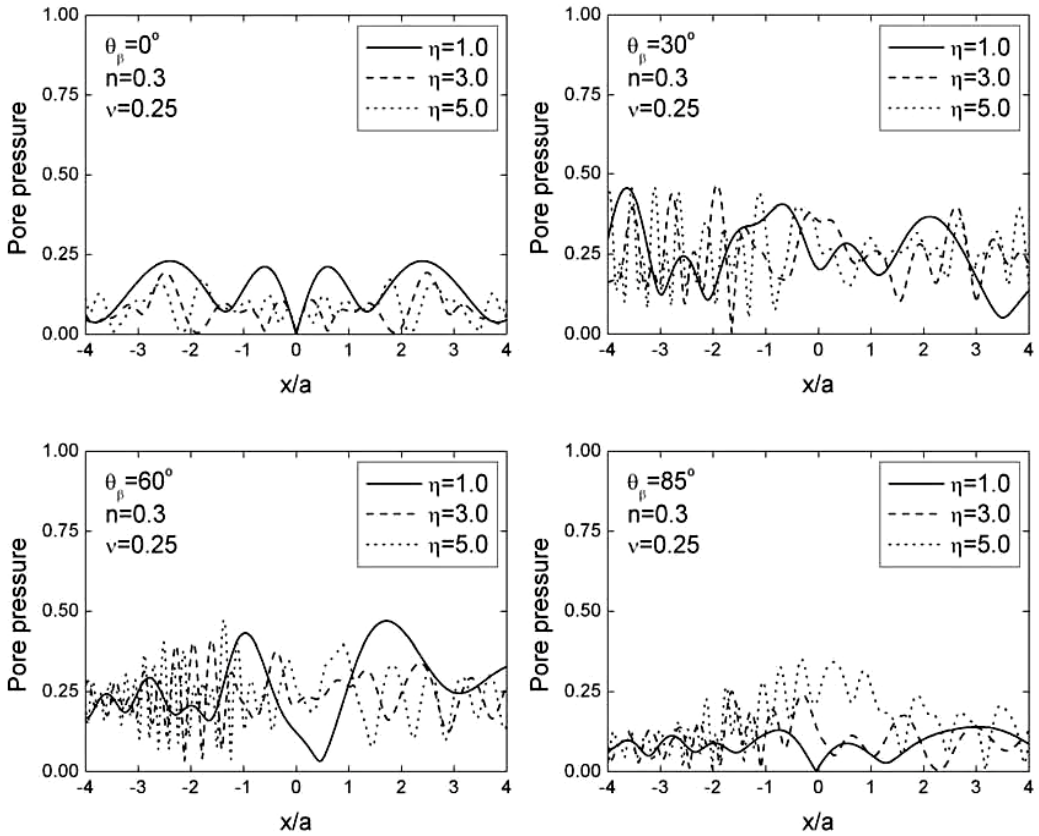

Fig. 20 Pore pressure along surface of half-space versus porosity (n = 0.3)

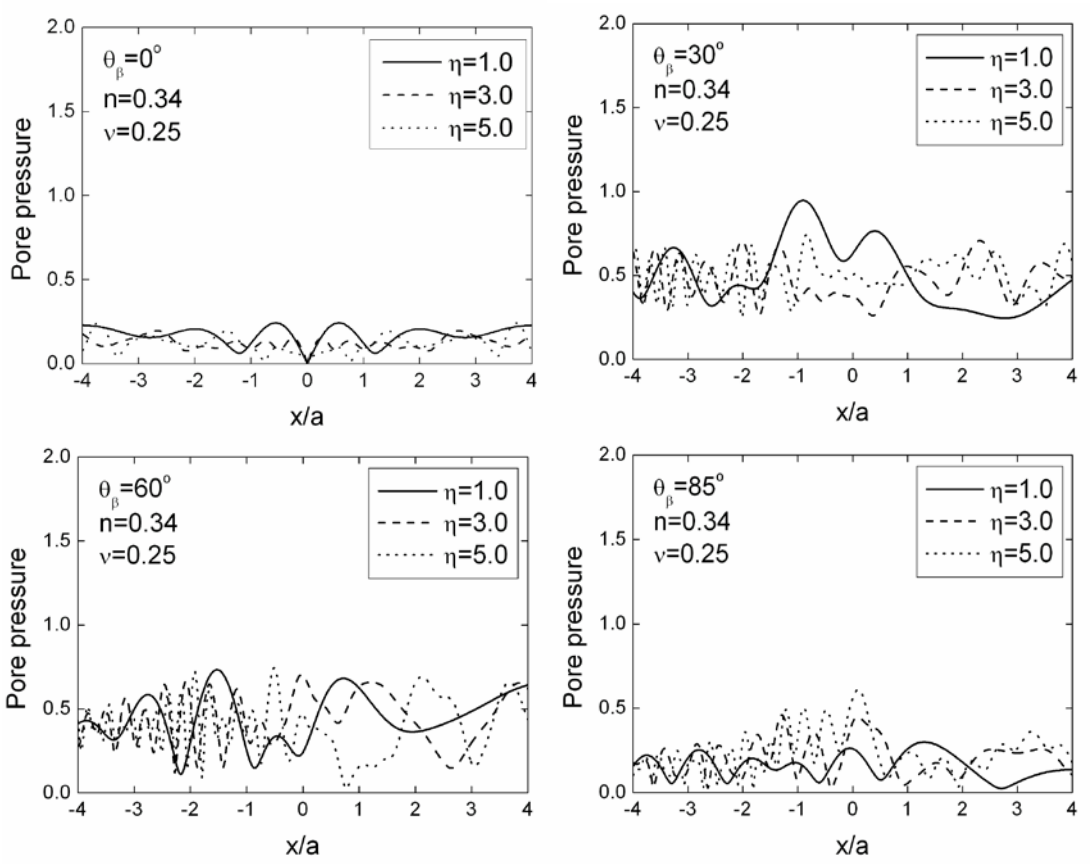

Fig. 21 Pore pressure along surface of half-space versus porosity (n = 0.34)

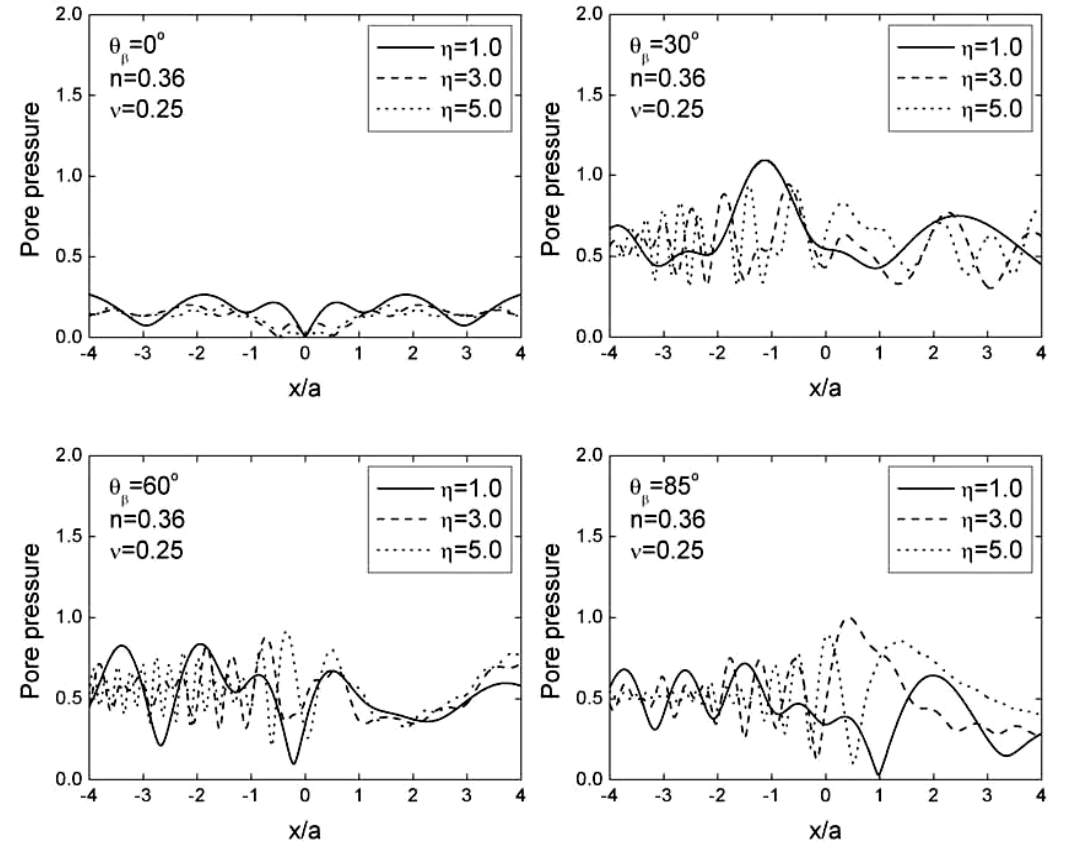

Fig. 22 Pore pressure along surface of half-space versus porosity (n = 0.36)

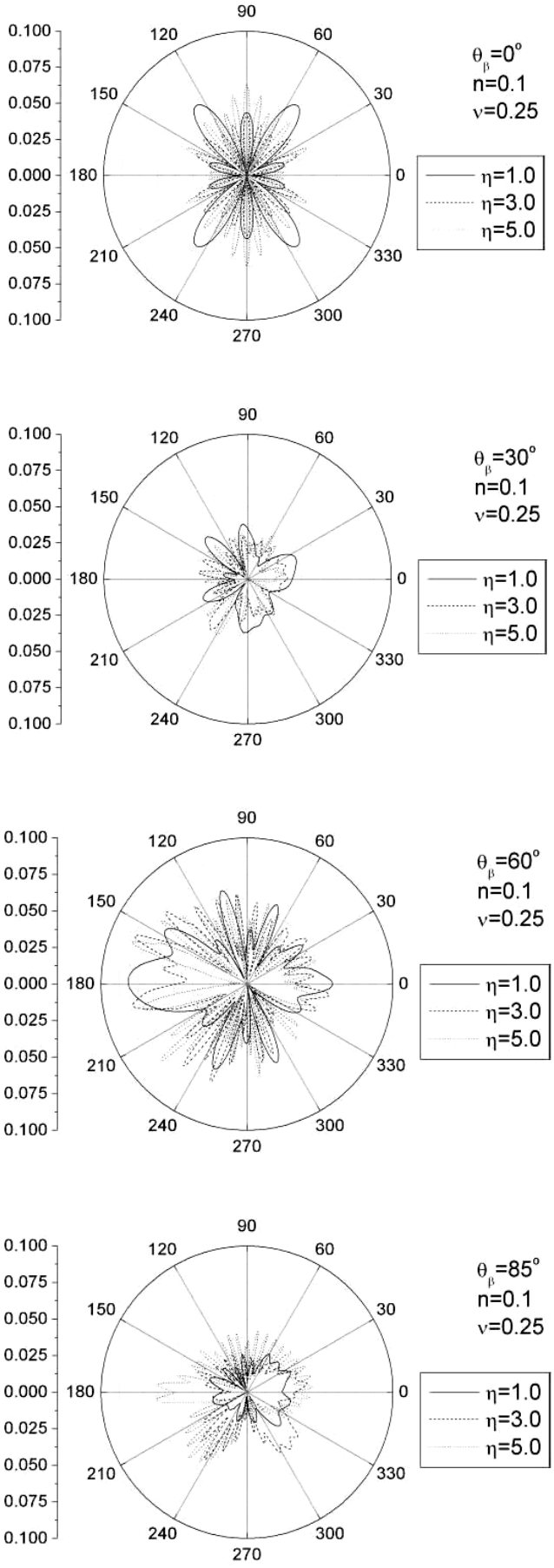

Fig. 23 Pore pressure along surface of cavity versus porosity (n = 0.1)

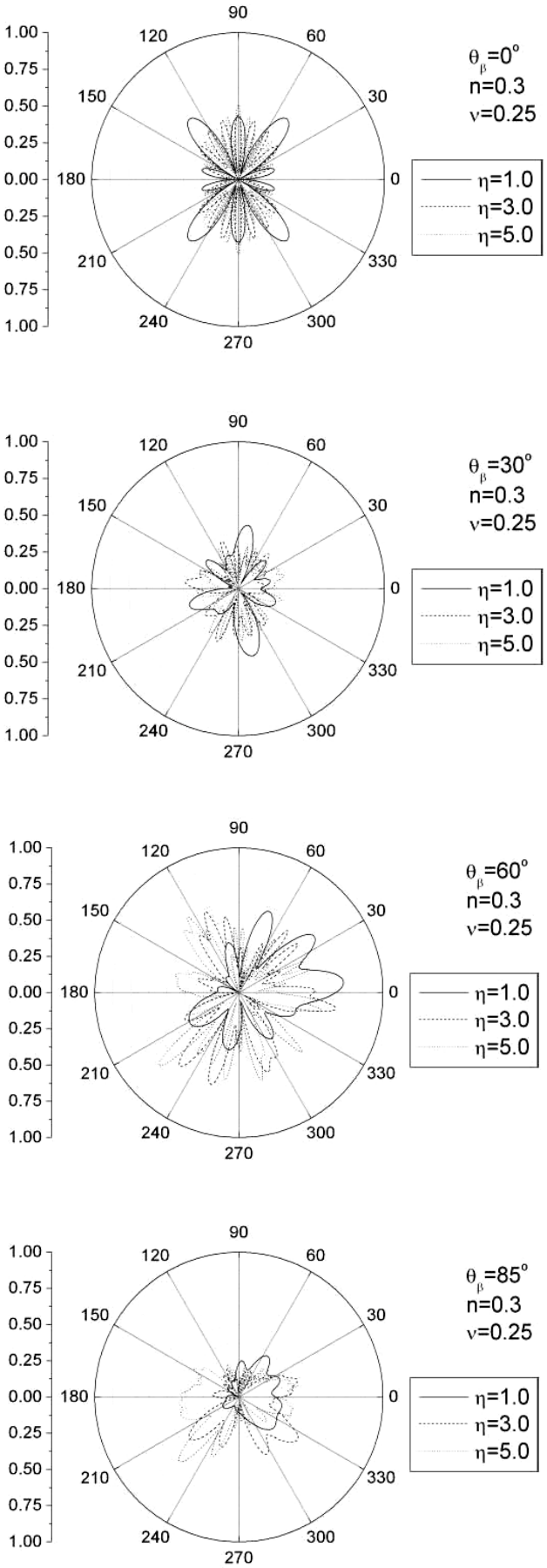

Fig. 24 Pore pressure along surface of cavity versus porosity (n = 0.3)

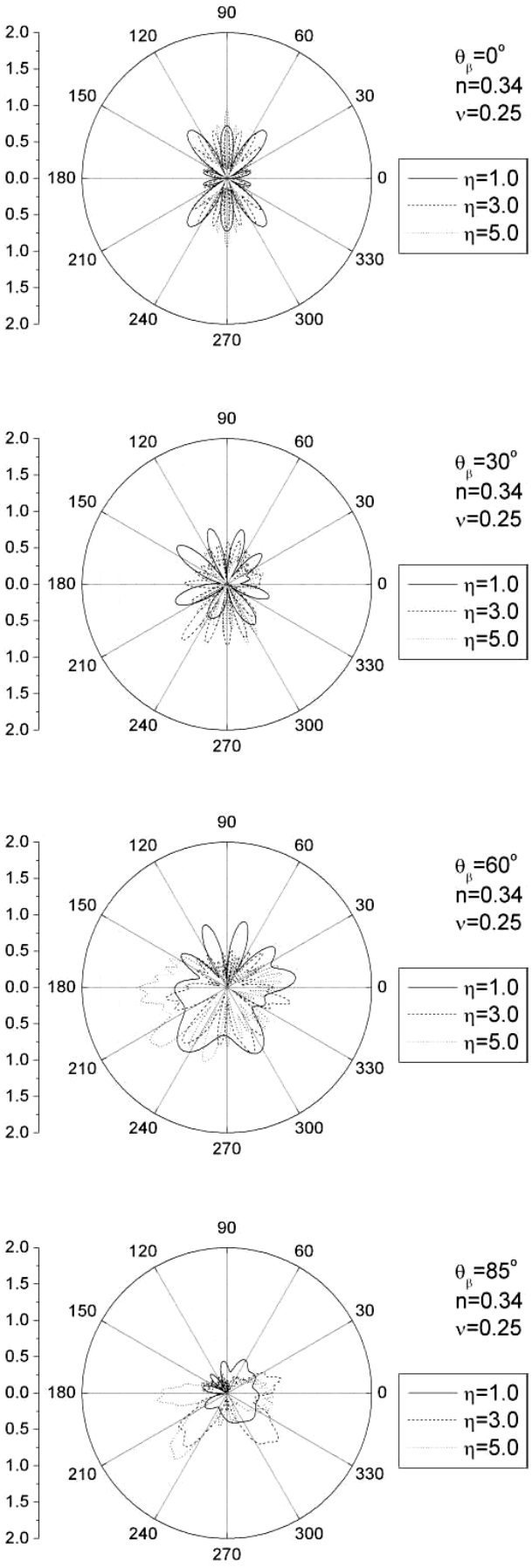

Fig. 25 Pore pressure along surface of cavity versus porosity (n = 0.34)

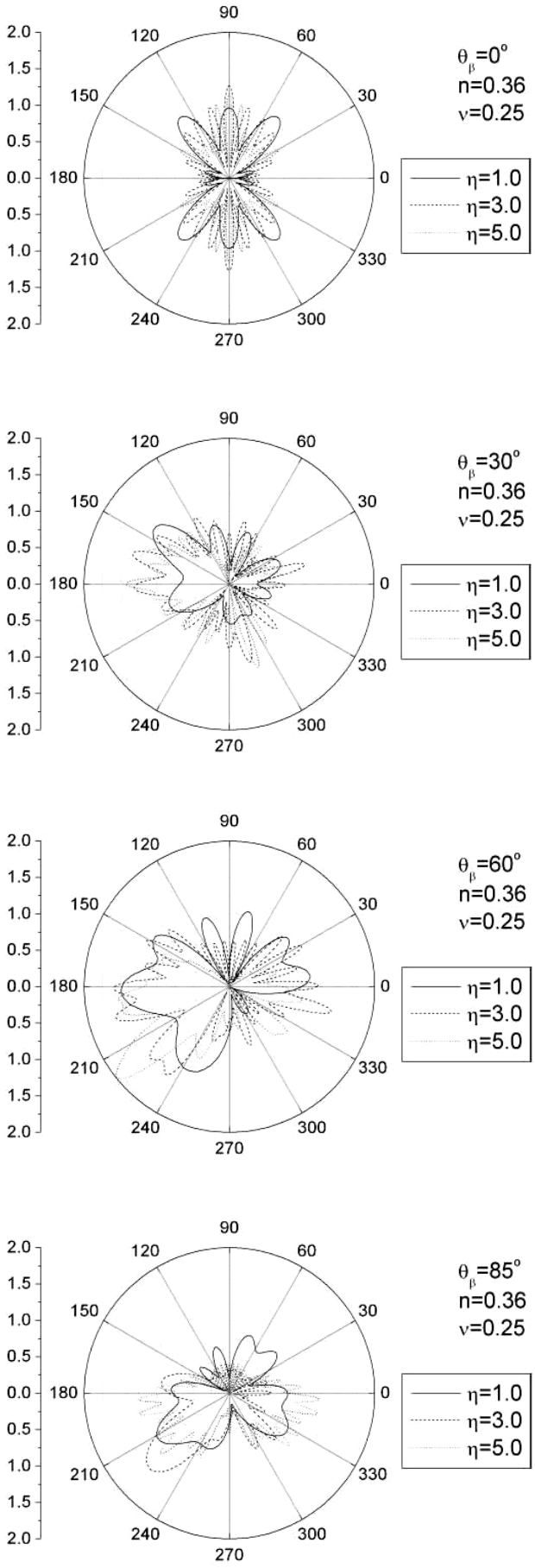

Fig. 26 Pore pressure along surface of cavity versus porosity (n = 0.36)

CONCLUSIONS

A wave-function series solution for the diffraction of incident plane SV waves by an underground circular cavity in a saturated poroelastic half-space was derived, and the effects of the incident frequencies, incident angles, boundary drainage, porosity, and Poisson's ratio on the diffraction of incident plane SV waves were illustrated.

It has been shown here that

- Depending on the incident angles, the surface displacement amplitudes near the cavity in a dry poroelastic half-space and in saturated poroelastic half-spaces can be very different and large phase shifts can be observed. The wavelengths of the waves in the undrained saturated poroelastic medium are slightly longer than those in the drained saturated poroelastic medium.
- The surface displacement amplitudes of the undrained saturated poroelastic half-space are close to those of the drained saturated poroelastic half-space for low-frequency waves, but the difference becomes larger as the frequency of the incident waves increases.
- For small porosity, the surface displacement amplitudes of the saturated poroelastic half-spaces are almost identical to those of the dry poroelastic half-space.
- For small porosity, the drainage condition has little influence on the surface displacement amplitudes; but for large porosity, the effect of drainage condition becomes significant.
- For the same porosity, the surface displacement amplitudes near the cavity in the undrained saturated half-space are larger than those in the drained saturated half-space.
- Poisson's ratio affects the surface displacement amplitudes near the cavity, both in drained and undrained conditions, and greater effects are observed for the undrained saturated half-space than for the drained saturated half-space.
- Large pore pressures are observed near and around the cavity, and are influenced strongly by the incident angles.
- As the porosity increases, the pore pressures increase significantly but their oscillations become smoother, and as the dimensionless frequency increases, the pore pressures become more complicated.

ACKNOWLEDGEMENTS

The authors gratefully acknowledge the support by National Natural Science Foundation of China under Grant No. 50378063. The authors also appreciate very much the comments and suggestions from the reviewers.

REFERENCES

1. Berryman, J.G. (1980). "Confirmation of Biot's Theory", Applied Physics Letters, Vol. 34, No. 4, pp. 382–384.
2. Berryman, J.G. (1981). "Elastic Wave Propagation in Fluid-Saturated Porous Media", The Journal of the Acoustical Society of America, Vol. 69, No. 2, pp. 416–424.
3. Berryman, J.G. (1985). "Scattering by a Spherical Inhomogeneity in a Fluid-Saturated Porous Medium", Journal of Mathematical Physics, Vol. 26, No. 6, pp. 1408–1419.
4. Biot, M.A. (1956a). "The Theory of Propagation of Elastic Waves in a Fluid-Saturated Porous Solid: I. Low-Frequency Range", The Journal of the Acoustical Society of America, Vol. 28, No. 2, pp. 168–178.
5. Biot, M.A. (1956b). "The Theory of Propagation of Elastic Waves in a Fluid-Saturated Porous Solid: II. Higher-Frequency Range", The Journal of the Acoustical Society of America, Vol. 28, No. 2, pp. 179–191.
6. Biot, M.A. (1962). "Mechanics of Deformation and Acoustic Propagation in Porous Media", Journal of Applied Physics, Vol. 33, No. 4, pp. 1482–1498.

7. Biot, M.A. and Willis, D.G. (1957). "The Elastic Coefficients of the Theory of Consolidation", Journal of Applied Mechanics, Transactions of ASME, Vol. 24, No. 4, pp. 594–601.
8. Davis, C.A., Lee, V.W. and Bardet, J.P. (2001). "Transverse Response of Underground Cavities and Pipes to Incident SV Waves", Earthquake Engineering & Structural Dynamics, Vol. 30, No. 3, pp. 383–410.
9. Deresiewicz, H. (1960). "The Effect of Boundaries on Wave Propagation in a Liquid-Filled Porous Solid: I. Reflection of Plane Waves at a Free Plane Boundary (Non-dissipative Case)", Bulletin of the Seismological Society of America, Vol. 50, No. 4, pp. 599–607.
10. Deresiewicz, H. (1961). "The Effect of Boundaries on Wave Propagation in a Liquid-Filled Porous Solid: II. Love Waves in a Porous Layer", Bulletin of the Seismological Society of America, Vol. 51, No. 1, pp. 51–59.
11. Deresiewicz, H. (1962). "The Effect of Boundaries on Wave Propagation in a Liquid-Filled Porous Solid: IV. Surface Waves in a Half-Space", Bulletin of the Seismological Society of America, Vol. 52, No. 3, pp. 627–638.
12. Deresiewicz, H. (1964a). "The Effect of Boundaries on Wave Propagation in a Liquid-Filled Porous Solid: VI. Love Waves in a Double Surface Layer", Bulletin of the Seismological Society of America, Vol. 54, No. 1, pp. 417–423.
13. Deresiewicz, H. (1964b). "The Effect of Boundaries on Wave Propagation in a Liquid-Filled Porous Solid: VII. Surface Waves in a Half-Space in the Presence of a Liquid Layer", Bulletin of the Seismological Society of America, Vol. 54, No. 1, pp. 425–430.
14. Deresiewicz, H. (1965). "The Effect of Boundaries on Wave Propagation in a Liquid-Filled Porous Solid: IX. Love Waves in a Porous Internal Stratum", Bulletin of the Seismological Society of America, Vol. 55, No. 5, pp. 919–923.
15. Deresiewicz, H. and Levy, A. (1967). "The Effect of Boundaries on Wave Propagation in a Liquid-Filled Porous Solid: X. Transmission through a Stratified Medium", Bulletin of the Seismological Society of America, Vol. 57, No. 3, pp. 381–391.
16. Deresiewicz, H. and Rice, J.T. (1962). "The Effect of Boundaries on Wave Propagation in a Liquid-Filled Porous Solid: III. Reflection of Plane Waves at a Free Plane Boundary (General Case)", Bulletin of the Seismological Society of America, Vol. 52, No. 3, pp. 595–625.
17. Deresiewicz, H. and Rice, J.T. (1964). "The Effect of Boundaries on Wave Propagation in a Liquid-Filled Porous Solid: V. Transmission across a Plane Interface", Bulletin of the Seismological Society of America, Vol. 54, No. 1, pp. 409–416.
18. Deresiewicz, H. and Skalak, R. (1963). "On Uniqueness in Dynamic Poroelasticity", Bulletin of the Seismological Society of America, Vol. 53, No. 4, pp. 783–788.
19. Deresiewicz, H. and Wolf, B. (1964). "The Effects of Boundaries on Wave Propagation in a Liquid-Filled Porous Solid: VIII. Reflection of Plane Waves at an Irregular Boundary", Bulletin of the Seismological Society of America, Vol. 54, No. 5, pp. 1537–1561.
20. Lee, V.W. and Cao, H. (1989). "Diffraction of SV Waves by Circular Cylindrical Canyons of Various Depths", Journal of Engineering Mechanics, ASCE, Vol. 115, No. 9, pp. 2035–2056.
21. Lee, V.W. and Karl, J. (1992). "Diffraction of SV Waves by Underground, Circular Cylindrical Cavities", Soil Dynamics and Earthquake Engineering, Vol. 11, No. 8, pp. 445–456.
22. Lee, V.W. and Karl, J. (1993). "Diffraction of Elastic Plane P Waves by Circular, Underground Unlined Tunnels", European Earthquake Engineering, Vol. VI, No. 1, pp. 29–36.
23. Lee, V.W. and Trifunac, M.D. (1979). "Response of Tunnels to Incident SH-Waves", Journal of the Engineering Mechanics Division, Proceedings of ASCE, Vol. 105, No. EM4, pp. 643–659.
24. Liang, J., Ba, Z. and Lee, V.W. (2006a). "Diffraction of Plane SV Waves by a Shallow Circular-Arc Canyon in a Saturated Poroelastic Half-Space", Soil Dynamics and Earthquake Engineering, Vol. 26, No. 6-7, pp. 582–610.
25. Liang, J., You, H. and Lee, V.W. (2006b). "Scattering of SV Waves by a Canyon in a Fluid-Saturated, Poroelastic Layered Half-Space, Modeled Using the Indirect Boundary Element Method", Soil Dynamics and Earthquake Engineering, Vol. 26, No. 6-7, pp. 611–625.

26. Lin, C.H., Lee, V.W. and Trifunac, M.D. (2005). "The Reflection of Plane Waves in a Poroelastic Half-Space Fluid Saturated with Inviscid Fluid", Soil Dynamics and Earthquake Engineering, Vol. 25, No. 3, pp. 205–223.
27. Pao, Y.H. and Mow, C.C. (1973). "Diffraction of Elastic Waves and Dynamics Stress Concentrations", Crane, Russak & Company, Inc., New York, U.S.A.
28. Paul, S. (1976a). "On the Displacements Produced in a Porous Elastic Half-Space by an Impulsive Line Load", Pure and Applied Geophysics, Vol. 114, No. 4, pp. 605–614.
29. Paul, S. (1976b). "On the Disturbance Produced in a Semi-Infinite Poroelastic Medium by a Surface Load", Pure and Applied Geophysics, Vol. 114, No. 4, pp. 615–627.
30. Philippacopoulos, A.J. (1988). "Lamb's Problem for Fluid-Saturated, Porous Media", Bulletin of the Seismological Society of America, Vol. 78, No. 2, pp. 908–923.
31. Philippacopoulos, A.J. (1997). "Buried Point Source in a Poroelastic Halfspace", Journal of Engineering Mechanics, ASCE, Vol. 123, No. 8, pp. 860–869.
32. Philippacopoulos, A.J. (1998). "Spectral Green's Dyadic for Point Sources in Poroelastic Media", Journal of Engineering Mechanics, ASCE, Vol. 124, No. 1, pp. 24–31.
33. Prevost, J.H. (1985). "Wave Propagation in Fluid-Saturated Porous Media: An Efficient Finite Element Procedure", International Journal of Soil Dynamics and Earthquake Engineering, Vol. 4, No. 4, pp. 183–202.
34. Prevost, J.H. (1987). "Mechanics of Continuous Porous Media", International Journal of Engineering Science, Vol. 18, No. 6, pp. 787–800.
35. Santos, J.E. (1986). "Elastic Wave Propagation in Fluid-Saturated Porous Media, I: The Existence and Uniqueness Theorems", RAIRO Mathematical Modelling and Numerical Analysis, Vol. 20, No. 1, pp. 113–128.
36. Santos, J.E. and Orena, E.J. (1986). "Elastic Wave Propagation in Fluid-Saturated Porous Media, II: The Galerkin Procedures", RAIRO Mathematical Modelling and Numerical Analysis, Vol. 20, No. 1, pp. 129–139.
37. Santos, J.E., Douglas, J., Corbero, J.M. and Lovera, O.M. (1990). "A Model for Wave Propagation in a Porous Medium Saturated by a Two-Phase Fluid", The Journal of the Acoustical Society of America, Vol. 87, No. 4, pp. 1439–1448.
38. Santos, J.E., Corbero, J.M., Ravazzoli, C.L. and Hensley, J.L. (1992). "Reflection and Transmission Coefficients in Fluid-Saturated Porous Media", The Journal of the Acoustical Society of America, Vol. 91, No. 4, pp. 1911–1923.
39. Senjuntichai, T. and Rajakapse, R.K.N.D. (1994). "Dynamic Green's Function of a Homogeneous Poroelastic Half-Plane", Journal of Engineering Mechanics, ASCE, Vol. 120, No. 11, pp. 2381–2403.
40. Theodorakopoulos, D.D. (2003a). "Dynamic Pressures on a Pair of Rigid Walls Retaining Poroelastic Soil", Soil Dynamics and Earthquake Engineering, Vol. 23, No. 1, pp. 41–51.
41. Theodorakopoulos, D.D. (2003b). "Dynamic Analysis of a Poroelastic Half-Plane Soil Medium under Moving Loads", Soil Dynamics and Earthquake Engineering, Vol. 23, No. 7, pp. 521–533.
42. Theodorakopoulos, D.D. and Beskos, D.E. (2003). "Dynamic Pressures on a Pair of Rigid Walls Experiencing Base Rotation and Retaining Poroelastic Soil", Engineering Structures, Vol. 25, No. 3, pp. 359–370.
43. Theodorakopoulos, D.D., Chassiakos, A.P. and Beskos, D.E. (2001a). "Dynamic Pressures on Rigid Cantilever Walls Retaining Poroelastic Soil Media. Part I. First Method of Solution", Soil Dynamics and Earthquake Engineering, Vol. 21, No. 4, pp. 315–338.
44. Theodorakopoulos, D.D., Chassiakos, A.P. and Beskos, D.E. (2001b). "Dynamic Pressures on Rigid Cantilever Walls Retaining Poroelastic Soil Media. Part II. Second Method of Solution", Soil Dynamics and Earthquake Engineering, Vol. 21, No. 4, pp. 339–364.
45. Theodorakopoulos, D.D., Chassiakos, A.P. and Beskos, D.E. (2004). "Dynamic Effects of Moving Load on a Poroelastic Soil Medium by an Approximate Method", International Journal of Solids and Structures, Vol. 41, No. 7, pp. 1801–1822.

46. Todorovska, M.I. and Lee, V.W. (1991). "A Note on Scattering of Rayleigh Waves by Shallow Circular Canyons: Analytical Approach", Bulletin of Indian Society of Earthquake Technology, Vol. 28, No. 2, pp. 1–16.
47. Vardoulakis, I. and Beskos, D.E. (1986). "Dynamic Behavior of Nearly Saturated Porous Media", Mechanics of Materials, Vol. 5, No. 1, pp. 87–108.
48. Yang, J. and Sato, T. (2001). "Analytical Study of Saturation Effects on Seismic Vertical Amplification of a Soil Layer". Geotechnique, Vol. 51, No. 2, pp. 161–165.
49. Zienkiewicz, O.C. and Shiomi, T. (1984). "Dynamic Behavior of Saturated Porous Media: The Generalized Biot Formulation and Its Numerical Solution", International Journal for Numerical and Analytical Methods in Geomechanics, Vol. 8, No. 1, pp. 71–96.
50. Zienkiewicz, O.C., Chang, C.T. and Battess, P. (1980). "Drained, Undrained, Consolidating, and Dynamic Behaviour Assumptions in Soils, Limits of Validity", Geotechnique, Vol. 30, No. 11, pp. 385–395.